**Volumetric yield sensing in a combine harvester**

by

**Michael Thomas Hanigan**

A thesis submitted to the graduate faculty

in partial fulfillment of the requirements for the degree of

MASTER OF SCIENCE

Major: Agricultural and Biosystems Engineering

Program of Study Committee:
Matthew Darr, Major Professor
Steven Hoff
Lie Tang

The student author, whose presentation of the scholarship herein was approved by the program of study committee, is solely responsible for the content of this thesis. The Graduate College will ensure this thesis is globally accessible and will not permit alterations after a degree is conferred.

Iowa State University

Ames, Iowa

2018

# TABLE OF CONTENTS

# LIST OF FIGURES

# LIST OF TABLES

# LIST OF EQUATIONS

## ACKNOWLEDGMENTS

First and foremost, I would like to thank God for my faith and the health of my family. I would like to give a special thanks to my family. Without their loving support and understanding, this opportunity would have not been achievable. I am forever grateful for everything that they have done for me.

I would like to thank Deere and Company for their financial support in pursuing my graduate degree. I owe a special thanks to Dr. Matthew Darr and Iowa State University for the extraordinary research opportunity they provided to me. I also wish to acknowledge Dr. Steven Hoff and Dr. Lie Tang for their guidance throughout my graduate degree.

Finally, I would like to express my appreciation to all my colleagues at Iowa State University. I am extremely grateful for their help and support throughout my research. Their assistance did not go unnoticed and my research would not have been possible without them. Thank you.

## ABSTRACT

This study focused on quantifying the engineering drivers for improving the accuracy of an optical beam-based yield monitor. The development of the single paddle test stand led to the quantification of the relationship between the output response of an optical beam-based mass flow sensor and a corresponding mass of grain traveling on an individual clean grain elevator paddle. The study optimized the design of the clean grain elevator paddle to reduce the variation in the output response from an optical beam-based mass flow sensor. The optimal location and adequate sampling frequency of the optical beam-based mass flow sensor, determined using the single paddle test stand, led to the development of two mass flow yield monitor algorithms. The study evaluated the two mass flow yield monitor algorithms against the Ag Leader and Raven Industries yield monitors. The results concluded that by applying a mass flow yield monitor algorithm utilizing a piecewise regression rather than a completely linear regression, a significant amount of error could be reduced across mass flow rates.

# CHAPTER 1. INTRODUCTION

## Project Description

With three consecutive years of decline in profits in the farm sector, data driven decisions have become more pivotal to help produce higher returns on investments for producers (USDA ERS, 2017). The producers of today rely on precision agriculture technologies, such as yield monitors, to provide them with the opportunity to better manage their farming operation. In the past two decades, precision agriculture has evolved and data driven decisions have become a must. The data produced from yield monitors is taken as the producers' ground truth and is used to drive numerous financial decisions that they will make over the next year from grain marketing, to seed variety selection, to fertilizer prescriptions. Inaccuracies in yield data can lead to incorrect management decisions by the producer.

Today's yield monitors can provide overall accuracies within a few percent, when properly calibrated (Darr, 2016). However, they are highly susceptible to increasing error due to the crop properties shifting from the initial calibration. In addition, the calibration process for these yield monitors is time consuming and arduous.

The focus of this research was to investigate the application of optical beam-based mass flow sensor in a yield monitor. With understanding of the fundamental principles of volumetric yield sensing, the goal was to optimize the mass flow sensing system by addressing the mechanical design of system components in the clean grain elevator and the installation position of the optical beam sensors.

# CHAPTER 2. LITERATURE REVIEW

## Components of Combine Harvester

The basic concepts of farming have changed minimally throughout history. Farming still requires a producer to plant a seed, care for it throughout the year, and a crop to be harvested at the end of the year. In order to improve productivity and efficiency for the producer, many mechanical innovations were created over time, like the combine harvester. The combine harvester takes the labor intensive tasks of cutting, threshing, separating, and cleaning of the crop and mechanizes them by system components (Figure 2.1).

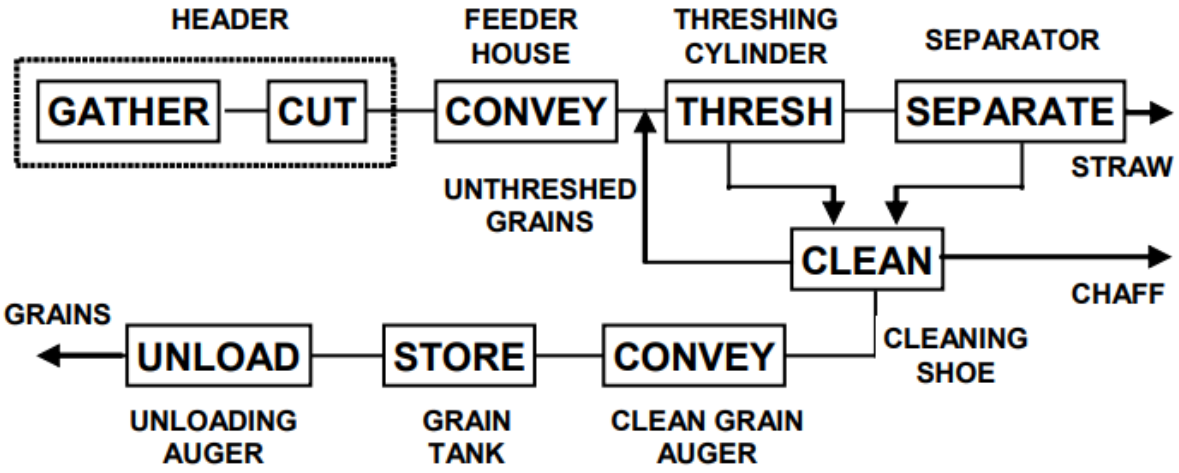


**Figure 2.1 : Functional process of components in combine harvester**

**Figure Credit: (Srivastava, 2006)**

Combine harvesters are equipped with crop specific headers that cut the crop and feed it into the feeder house. The feeder house conveys the crop into the threshing cylinder, or rotor, using a specially designed chain. Once the crop enters the threshing cylinder, the grain is dislodged from the plant material by shearing the crop between the rotating threshing cylinder and a set of metal grates, known as the concaves. The concaves are crop specific and the distance between them and the threshing cylinder is known as the concave clearance. The

concave clearance is often adjusted by the operator to optimize the threshing efficiency of the combine harvester. Following the threshing cylinder, large plant material is transferred out the back of the combine harvester, leaving the grain and smaller plant material commingled entering the cleaning shoe.

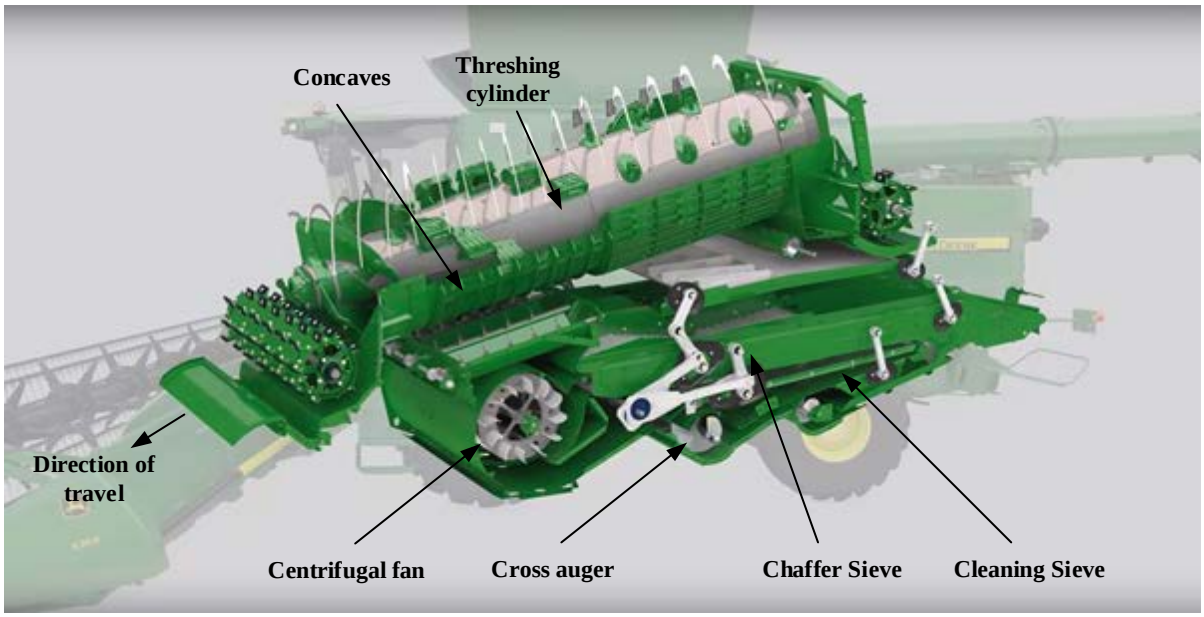


**Figure 2.2 : Components to combine harvester**

**Figure Credit: (John Deere, 2017)**

The cleaning shoe is where the final separation process tasks place. The cleaning shoe uses a centrifugal fan that blows air through a series of two highly engineered sieves toward the back of the machine. The top and bottom sieves are referred to as the chaffer sieve and the cleaning sieve, respectively (ASAE S343.4, 1970). The air blown by the centrifugal fan uses the rotational and lateral aerodynamic properties of the grain to optimize the finger-like design of the oscillating sieves to hold back the grain while forcing the remaining plant material out the back of the combine harvester. Each sieve's opening can be adjusted by the operator to minimize lost grain out the back of the machine and to improve the cleanliness of the grain. It is not uncommon that a portion of the grain still remains un-threshed. Any un-

threshed grain that is too dense to be forced out the back of the machine by blown air and large enough that it would not pass through the sieves is conveyed by the tailing elevator to be re-threshed. Once the grain is completely cleaned, it is conveyed by the horizontal cross auger to the clean grain elevator. The clean grain elevator vertically lifts the grain, using a paddle chain and fountain auger, into the grain tank (Figure 2.3).

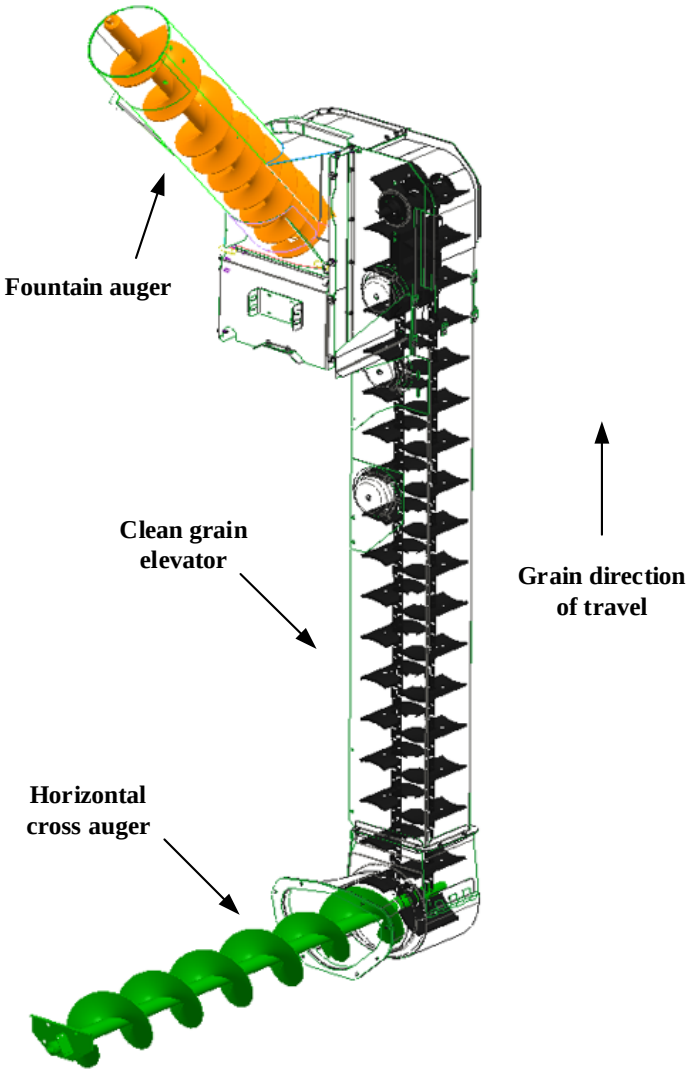


**Figure 2.3 : Clean grain conveying system**

## Measuring Crop Yield

The combine harvester also introduced another opportunity in crop harvesting, measuring crop performance throughout the field operation, known as crop yield. After the grain is completely cleaned in a combine harvester, there is an opportunity to quantify the performance of the crop. The system used to quantify the performance is called the yield monitor and was first successful introduced on the market by Al Myers in 1992 (Royer, 2017). A survey conducted by the United States Department of Agriculture exhibited that, over a 17 year period, the usage of a yield monitor and the usage of yield data to create a yield map increased on average by 3.3% and 2.0% per year, respectively (Figure 2.4).

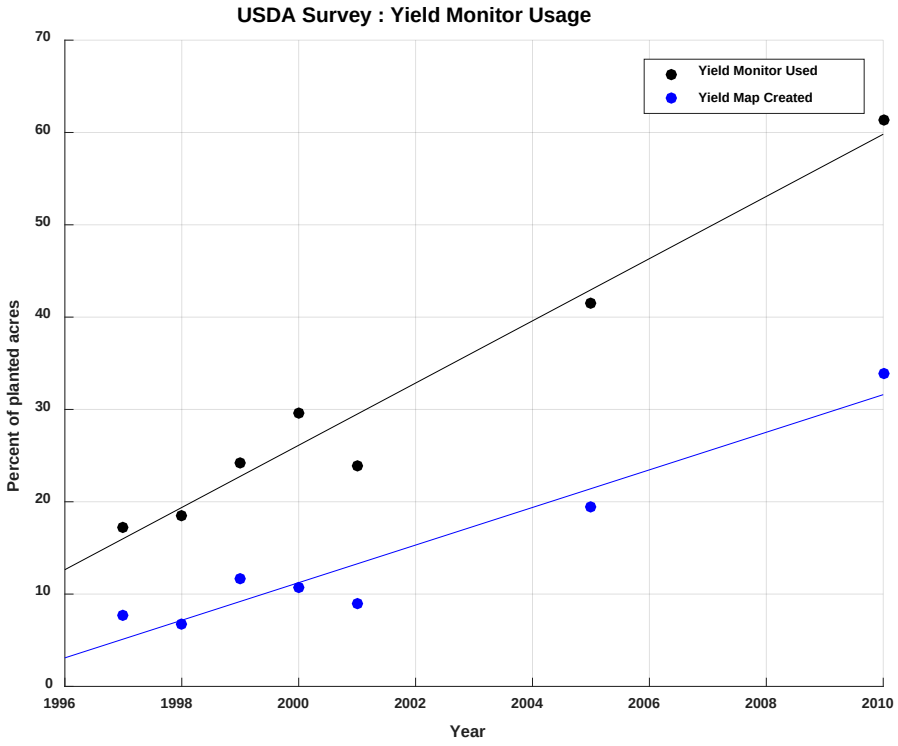


**Figure 2.4 : USDA survey yield monitor usage**

In order to produce yield data, the yield monitor consists of several sensing technologies including: a moisture sensor, a GPS receiver, a display, various secondary

sensors, and a mass flow sensor. Together, these technologies estimate yield on either a mass or volume per unit area basis (Table 2.1).

**Table 2.1 : Units of yield**

| Unit System | Dimensional Analysis | Units |
|---|---|---|
| US Customary | $L_1^3 * L_2^{-2}$ | Bushels / acre |
| International System of Units | $M * L^{-2}$ | Tonne / hectare |

**Moisture Sensor**

The ability to measure crop moisture content is a crucial part of yield monitoring. Traditional moisture sensors determine the moisture content of the grain using capacitive sensors located in a confined chamber in the sensor housing. In the chamber, two conductive plate are oriented opposed of one another. When grain is fed into the chamber from either the clean grain elevator or the fountain auger, an electric field is generated. Due to the dielectric properties of the grain, the output voltage from the capacitive sensor will vary based on the moisture content. The change in voltage is measured and then correlated to a known moisture content for each crop.

**Display and GPS Receiver**

The display, located in the operator station, provides an interactive user interface between the combine harvester and the operator. The display has the ability to present the yield map, store yield data, harvest setting, provide the operator with necessary sensor calibration functions, and alerts the operator with diagnostic messages.

Frequently, the display is linked to a global positioning system (GPS) receiver. The GPS receiver provides the yield monitor with the physical location and ground speed of the combine harvester in the field. The physical location and ground speed are used to link yield data points back to their physical location in the field. The synthesis of physical location data

and yield data points creates the yield map on the display. The yield map, provides a geographical representation of crop yield to the operator (Figure 2.5).

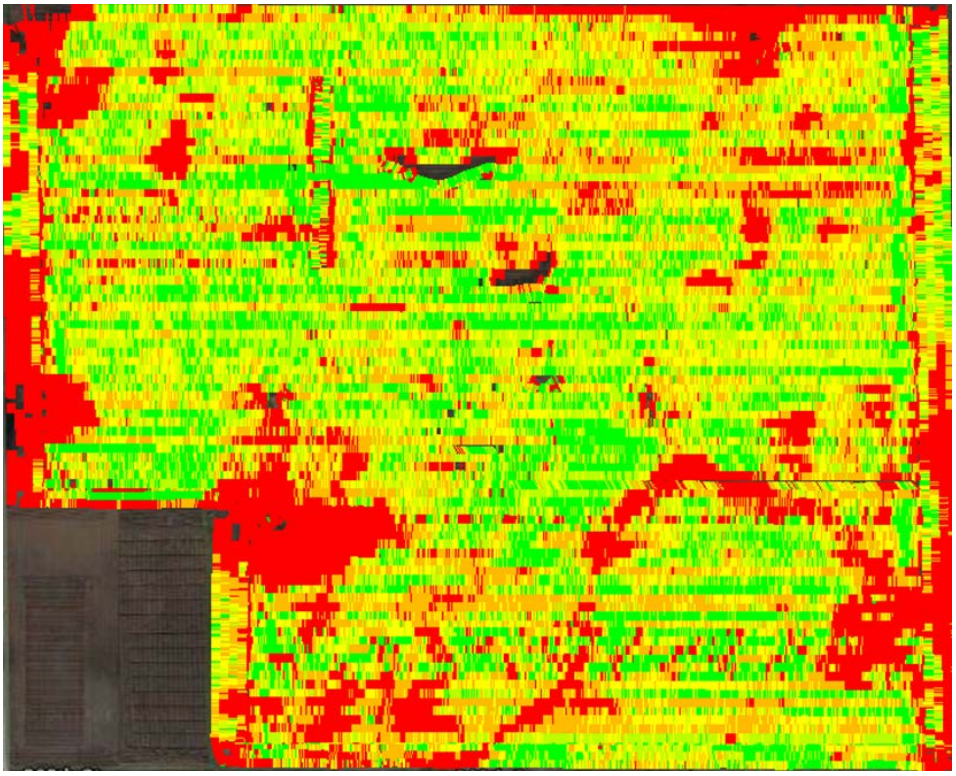

**Figure 2.5 : Crop yield map**

**Secondary Sensors**

In order to ensure high quality in the data collection process, numerous secondary sensors are used in conjunction with the GPS receiver to provide accurate yield mapping. The first of two notable sensors is the separator speed sensor. The separator speed sensor's function is to verify that the separation system of the combine harvester is engaged in harvest operation. The other notable secondary sensor is the header height sensor. The header height sensor indicates when the combine harvester enters or exits crop. This is an important function of starting and stopping yield mapping.

**Mass Flow Sensor**

The mass flow sensor in the yield monitor measures the instantaneous grain flow through the combine harvester. On the market today, producers have the opportunity to select from numerous types of mass flow sensors with the two most common being the impact-based sensors and the optical beam-based sensors. Radiation, electromagnetic, and metering-based systems are also available on the market as well.

**Table 2.2 : Mass flow sensor for combine harvester manufacturer**

| Combine Harvester Manufacturer | Yield Monitor Brand | Mass Flow Sensor |
|---|---|---|
| AGCO / Fendt / Massey Ferguson | Ag Leader | Impact-based |
| CLAAS / Lexion | CLAAS | Optical beam-based |
| CNH | Ag Leader | Impact-based |
| John Deere | Ag Leader | Impact-based |
| Tribine | Ag Leader | Impact-based |
| - | Ag Leader | Impact-based |
| - | Precision Planting | Impact-based |
| - | Raven Industries | Optical beam-based |
| - | Trimble | Optical beam-based |

**Impact-based sensors**

Impact-based sensors are the most common mass flow sensors on the market today (Table 2.2). Currently, the majority of equipment manufacturers come equipped with an Ag Leader impact-based mass flow sensor on their base combine harvester package. The Ag Leader impact-based mass flow sensor is commonly located adjacent to the clean grain elevator discharge in the transition housing (Figure 2.6). The Ag Leader impact-based mass flow sensor contains an impact plate mounted to a force transducer (McNaull, 2016). The force transducer converts the force, registered from the acceleration of grain that is discharged from the paddles of the clean grain elevator, to a mass flow rate based on a calibration completed by the operator.

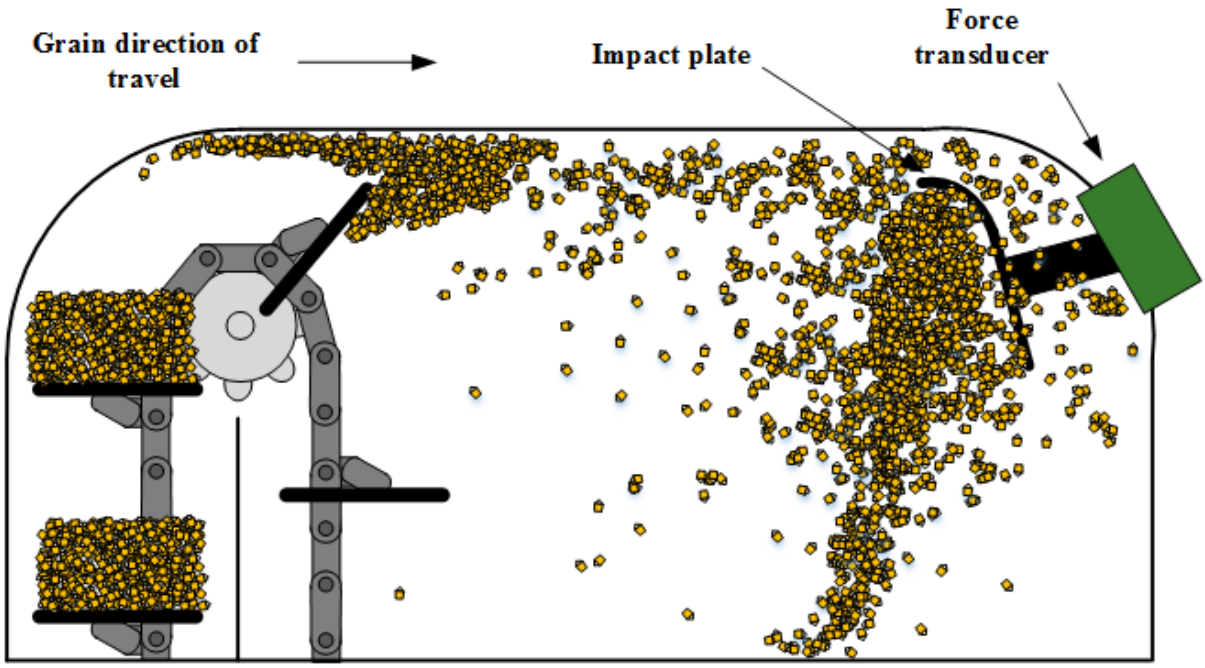


**Figure 2.6 : Ag Leader mass flow sensor**

Recently, Precision Planting introduced another impact-based mass flow sensor onto the market. It offers a unique location than that of the Ag Leader sensor (Figure 2.7). The Precision Planting mass flow sensor is located at the top of the clean grain elevator and is comprised of two Hall Effect sensors, which independently vary their output voltage based on the displacement of the impact plate. The displacement of the impact plate is the result of grain being released from the clean grain elevator paddle. The released grain is forced out against the housing of the clean grain elevator unit it contacts the impact plate, causing deflection. Similar to the Ag Leader mass flow sensor, the Precision Planting mass flow sensor output is converted to mass flow rate based on a calibration factor. Exclusive to Precision Planting, they determine the calibration factor for their impact-based mass flow sensor automatically by a crop properties bucket found in their engineered clean grain elevator chain (U.S. Patent No. 9,686,914).

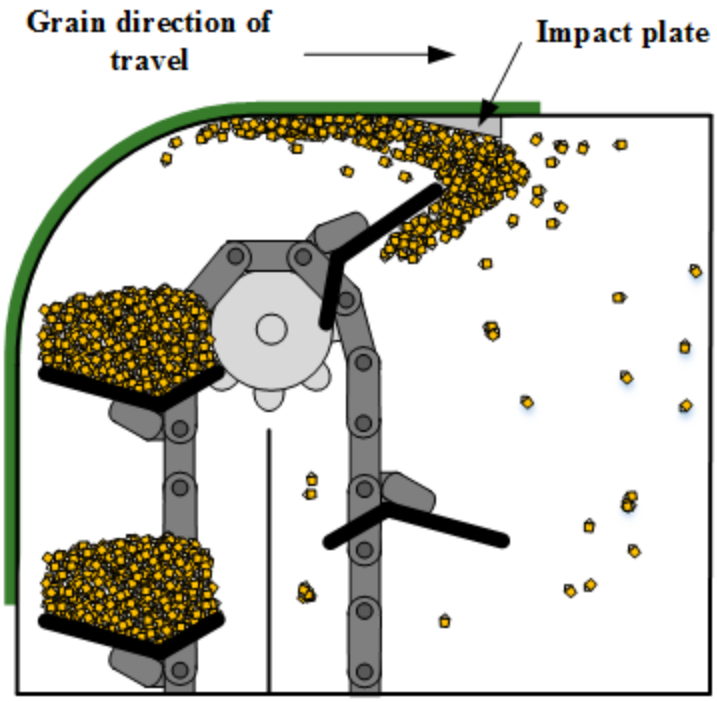


**Figure 2.7 : Precision Planting mass flow sensor**

**Optical beam-based sensors**

Optical beam-based mass flow sensors are another common sensing technology used to determine the mass flow of grain through a combine harvester. This non-contact technology comprises of a pair of opposed photoelectric sensors, an emitter and a receiver, rigidly fixed to the housing of the clean grain elevator. The emitter and receiver are positioned opposite of each other and perpendicular to the grain direction of travel in the clean grain elevator (Figure 2.8).

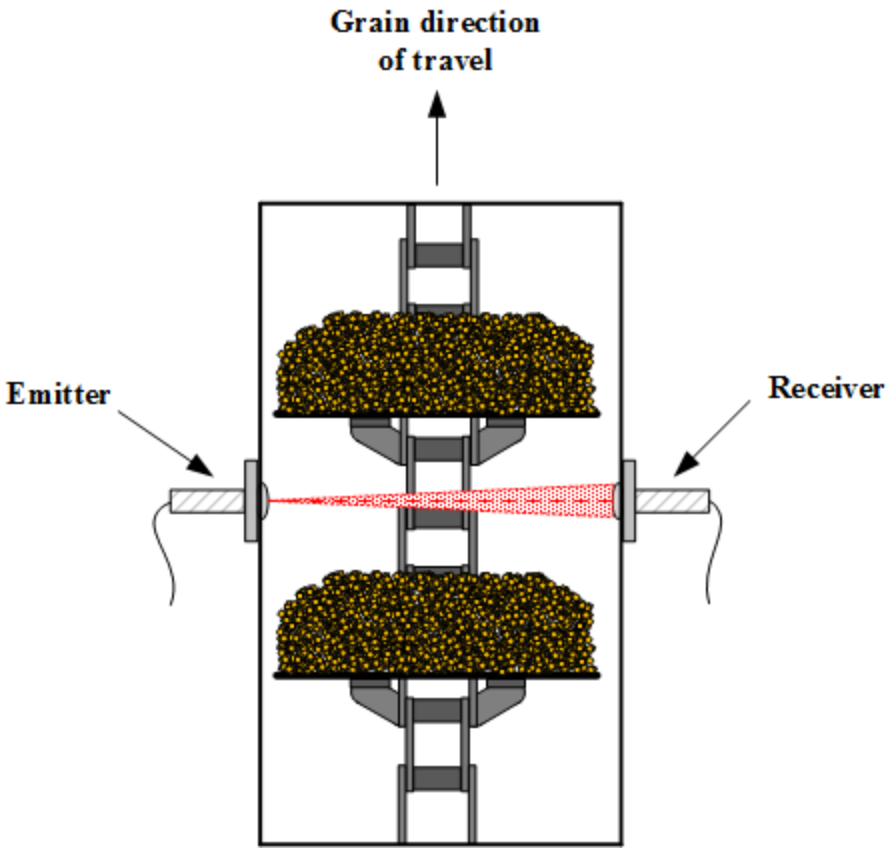


**Figure 2.8 : Optical beam-based mass flow sensor**

The emitter transmits a near infrared (NIR) beam of light across the clean grain elevator at the receiver. When the beam of light is unbroken, the receiver registers the emittance and outputs a high voltage response. Once the beam of light is broken between the emitter and receiver, the receiver is unable to sense any emittance and outputs a low voltage response. The duration of time that the response is at low voltage is then related to the additive height of both grain and the clean grain elevator paddle. In order to determine the height of only the grain on the clean grain elevator paddle, a zero calibration is conducted before there is any grain flow through the machine to determine the empty height of the clean grain elevator paddle, known as the tare value. After the calibration, the tare value is stored

and subtracted from the additive height, resulting in only the height of the grain (Equation 2.1). The grain height can then be used to determine mass flow rate (Equation 2.2).

**Equation 2.1 : Grain height estimation from optical beam-based mass flow sensor**

$$Grain\ height = Additive\ height - Tare\ value$$

**Equation 2.2 : Mass flow rate estimation from optical beam-based mass flow sensor**

$$Mass\ flow\ rate\ = \frac{Grain\ height}{Paddle} * \frac{Paddle}{sec} * Paddle\ area * Grain\ test\ weight$$

## Key Performance Factors to Optical Beam-Based Mass Flow Sensing

The accuracy and variability of yield monitors that use optical beam-based mass flow sensors can be driven back to the fundamental principles of the measurement collected. Optical beam-based mass flow sensors rely heavily on the duration of blocked time recorded to be an accuracy method of estimating the height of grain on a clean grain elevator paddle. However, this measurement can be influenced by three major divisions of factors: opposed photoelectric sensor factors, mechanical combine harvester factors, and environmental factors.

### Opposed Photoelectric Sensor Factors

Opposed photoelectric sensors are very common and their usages can be found in everyday life. The diversity of their application can vary from safety control systems on garage door openers to the detection of instantaneous events in control systems. The effectiveness of these sensors on detecting instantaneous events, like the height of grain on a

clean grain elevator paddle, can be attributed to the time delays of the output response time and the emitted beam pattern.

**ON/OFF time delays**

Every model of opposed photoelectric sensors has an associated ON/OFF time delay in its output response. In the application of using opposed photoelectric sensors to determine the height of grain on a clean grain elevator paddle, the actual height and the measured height will differ. The sensor measurement will include two time delays; one, from the receiver to record that the light beam was blocked (OFF) and another to record the reestablishment of emittance (ON). Understanding of these time delays is important to relating the measured height back to the actual. In addition, the sum of the ON and OFF time delays equals the minimum output duration that the receiver can achieve.

**Beam pattern**

Another principle of opposed photoelectric sensors that will attribute to the difference found in the actual and measured heights can be the result of the emitter's beam pattern. Beam patterns for opposed photoelectric sensors are generally conical in shape (Figure 2.9). The diameter of the beam pattern is a function of the distance between emitter and the receiver. Beam patterns are specific to each model of opposed photoelectric sensor, varying in distances and widths.

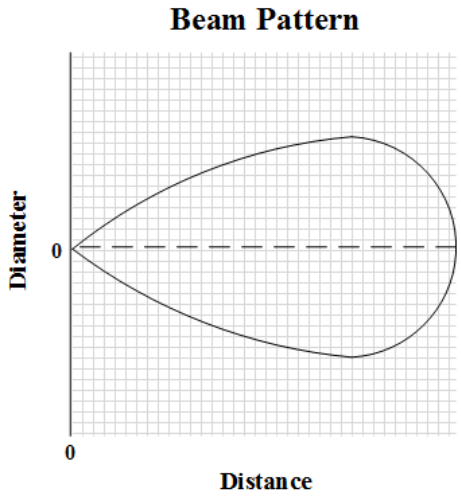


**Figure 2.9 : Opposed photoelectric emitter beam pattern**

The difference caused between the actual and measured heights is due to the relationship between the blockage point and the minimum emittance point. In order to experience complete lack of emittance, the entire available beam pattern must be completely blocked between the emitter and receiver (Figure 2.10). However, the receiver is able to detect emittance when the smallest amount of light is available for detection (Figure 2.11). This causes the receiver to record the measured height less than the actual.

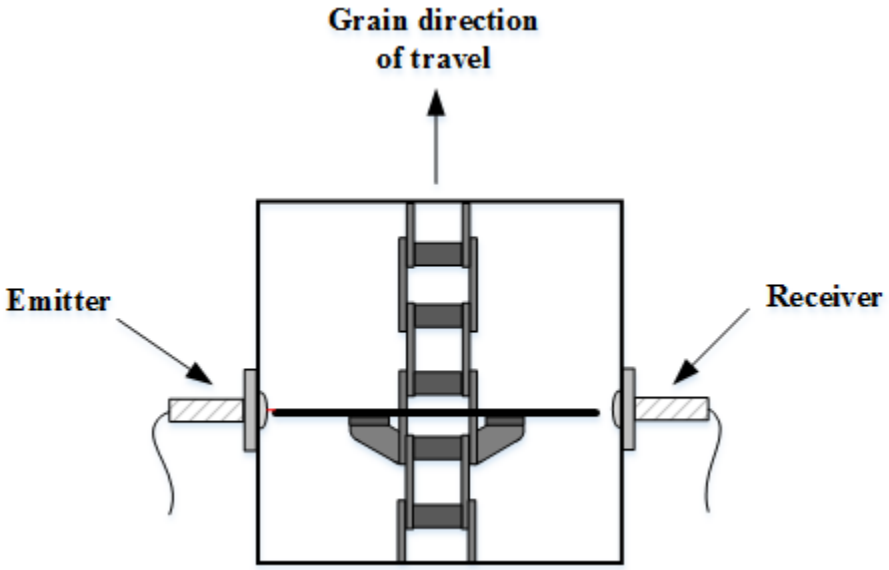


**Figure 2.10 : Complete lack of emittance**

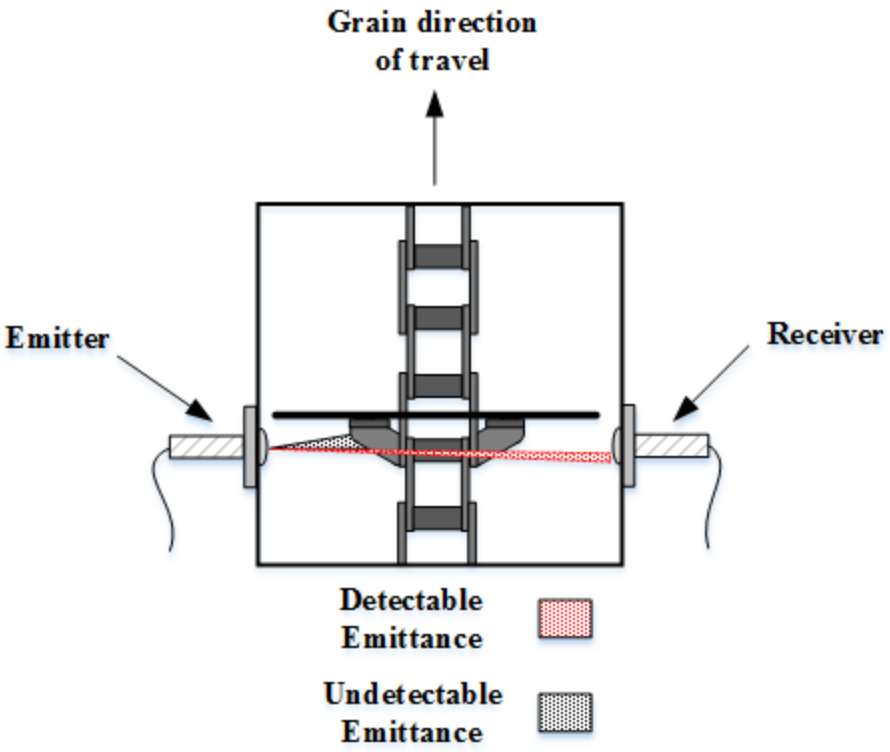


**Figure 2.11 : Minimum emittance**

Alignment of the pair is also extremely important to the receiver's ability to detect emittance. Misalignment shrinks the available beam pattern that the receiver is able to detect (Figure 2.12). In the application of measuring the height of grain on a paddle in the clean grain elevator, misalignment can shrink the beam pattern enough that the receiver becomes more susceptible to false ON/OFFs caused from free falling grain falling down the clean grain elevator.

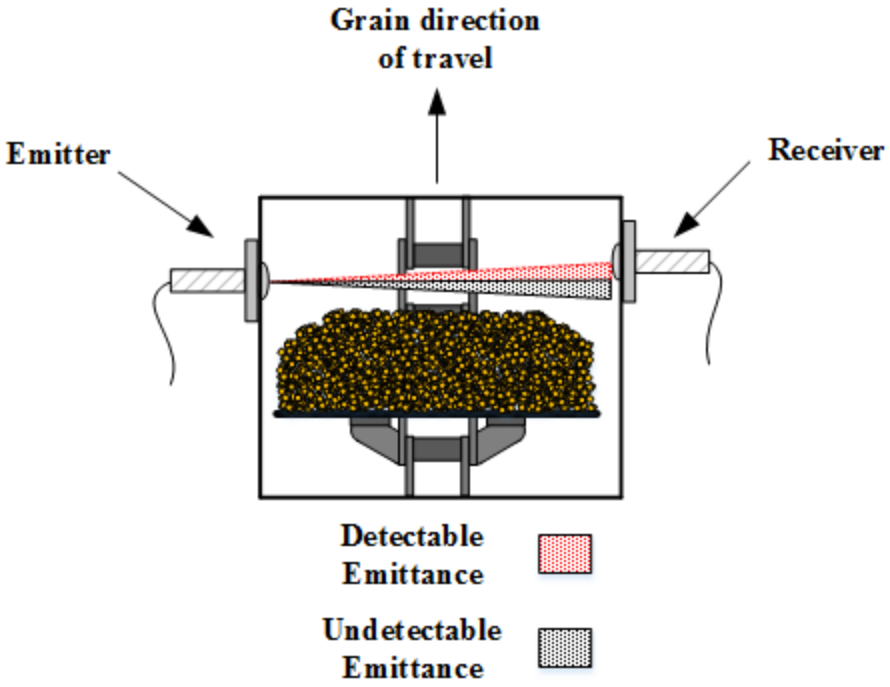


**Figure 2.12 : Misalignment effect on detectable emittance**

In order to help minimize misalignment, each opposed photoelectric sensor has a specially designed optical lens attached to the sensor face (Figure 2.13). During installation, each opposed photoelectric sensor is pressed against the outside of the clean grain elevator housing. The large outer diameter of the lens aids in positioning the opposed photoelectric sensor perpendicular to the clean grain elevator housing. In addition, each lens provides a durable clear cover over the face of the sensor to protect it from the harsh dynamic environment in the clean grain elevator.

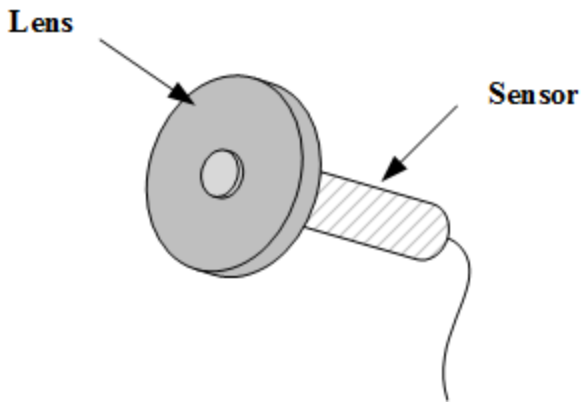


**Figure 2.13 : Opposed photoelectric sensor and lens**

**Mechanical Combine Harvester Factors**

As discussed prior, accurately relating the duration of block time to the height of only grain on the clean grain elevator paddle is a function the tare value (Equation 2.1). The inability to accurately and consistently determine the tare value can introduce variation directly into the grain height measurement. Further, if the determined tare value fluctuates from what it actually representation in the overall height measurement, it will also introduce error.

**Clean grain elevator speed**

Because the clean grain elevator speed is used directly to relate the blockage time to the grain height measurement, the ability to accurately estimate it is imperative to the performance of optical beam-based mass flow sensing. Any deviation found in the clean grain elevator speed measurement can lead to error and variation in the grain height measurement. Commonly, the clean grain elevator speed is determined by a sensor attached to the end of the horizontal cross auger. The sensor records the pulses caused by the rotation of a tone wheel, which can be translated to revolutions per minute and reported out over the controller area network (CAN).

**Clean grain elevator chain tension**

Due to the output measurement of receiver being a linear line between the blockage point and minimum emittance point, maintaining the proper chain tension in the clean grain elevator is important. When chain tension decreases below the design threshold, the clean grain elevator chain and paddles have the opportunity to oscillate in the clean grain elevator (Figure 2.14). This oscillation can cause the measurement point to vary from that of the tare value on the clean grain elevator paddle, adding error and variability into the measurement. CLAAS, a combine harvester manufacturer that uses optical beam-based mass flow sensing, equips their clean grain elevator with a hydraulic chain tensioner to minimize the opportunity of improper chain tension in their system.

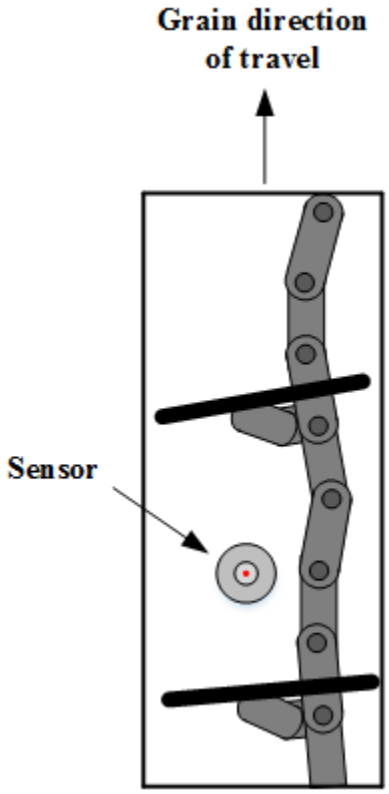


**Figure 2.14 : Result of improper clean grain elevator chain tension**

### Clean grain elevator paddle

Similar to maintaining proper clean grain elevator chain tension, any part of the clean grain elevator paddle that introduces variation into the tare value can lead to error. Because the blockage point is a function of the amount of grain on the clean grain elevator paddle, any mechanical components that dictate the ability to sense the amount of grain is not ideal. Additionally, the point of minimum emittance needs to be the controlled to maintain the same measurement point for every clean grain elevator paddle, every time.

## Environmental Factors

While combine harvesting, there are numerous uncontrollable environmental, non-mechanical, factors that influence the performance of optical beam-based mass flow sensors. These factors include elements that change the grain presentation to the sensor.

### Machine orientation

Cropland slopes can cause the combine harvester's orientation to change during harvesting operation. Changes in the machine orientation are generally designated by two dimensional angles, pitch and roll. Machine pitch refers to the fore and aft rotation of the machine between the front and rear axles. Pitch is ordinarily the result of harvesting up or down hills. Machine roll, caused by harvesting on side slopes, is attributed to the rotation between the right and left tires on the same axle plane (Figure 2.15).

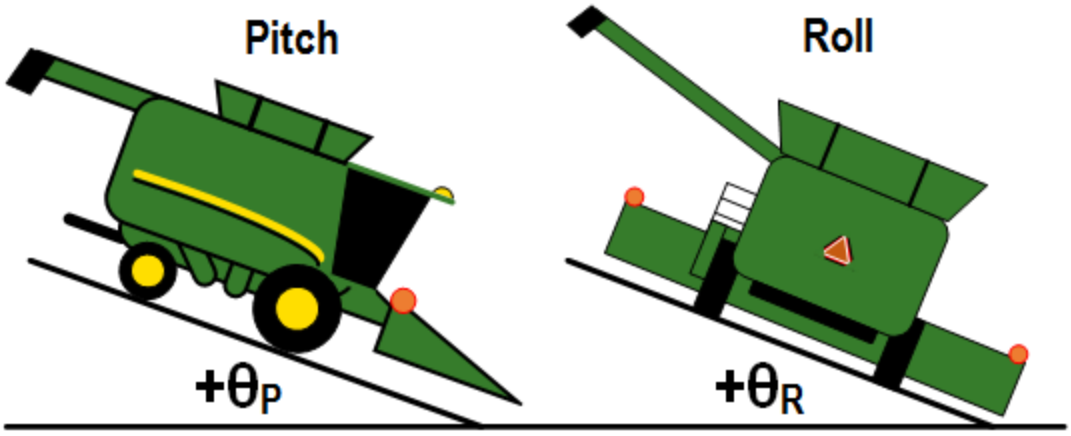


**Figure 2.15 : Machine orientation**

**Figure Credit: (Schuster, 2016)**

Consequently, when the orientation of the machine changes, the sensing environment in clean grain elevator changes with it. Machine orientation changes can causes uneven loading on the clean grain elevator paddles. The uneven loading presents a skewed representation of the actual amount of grain on the paddle to the sensor. This skewness was proven to be statistically significant when comparing machine orientation and the yield estimation error of an optical beam-based yield monitor (Schuster, 2016).

**Grain test weight**

Optical beam-based mass flow sensors relate their volumetric flow rate measurement to mass flow rate by multiplying the volumetric flow rate with the grain test weight. Grain test weight is a bulk density measurement of the clean grain sample and is commonly reported in pounds per bushel in the US customary unit system. Grain test weight can be effected by grain moisture content, granular size and shape, and material other than grain. Current combine harvesters are not equipped to determine the instantaneously grain test weight during harvesting operation. In order to avoid skewness in the yield data, volumetric yield monitors utilize a calibration to compensate for the inability to measure the grain test

weight. According to Blackmore in 1999, volumetric yield monitors should be calibrated and re-calibrated several times per day to provide accurate yield data.

**Table 2.3 : U.S. Grades and grade requirements for corn**

| Grade | Minimum test weight (pounds per bushel) | Maximum limits of: | |
|---|---|---|---|
| | | Total damaged kernels (percent) | Broken corn and foreign material (percent) |
| U.S. No. 1 | 56.0 | 3.0 | 2.0 |
| U.S. No. 2 | 54.0 | 5.0 | 3.0 |
| U.S. No. 3 | 52.0 | 7.0 | 4.0 |
| U.S. No. 4 | 49.0 | 10.0 | 5.0 |
| U.S. No. 5 | 46.0 | 15.0 | 7.0 |

## U.S. Patent Review

**U.S. Patent No. 6,282,967**

CLAAS claims the invention of an apparatus that has the ability to measure the throughput of material on a conveyer. Using three photoelectric devices, CLAAS claims the ability to accurately determine the volume of material being continuously conveyed on blades moving in a conveyer shaft. The first photoelectric device is mounted so that its light beam output is parallel to the surfaces of the blades. A processor, which has the capacity to determine the distance between the top edge of the conveyed material and the passing conveyer blade via light-dark periods in the output signal, is said to compensate for the thickness of the blades and the blade spacing in order to determine the volume of the material on the blade. Photoelectric devices two and three are claimed to be mounted at right angles to the first photoelectric device (Figure 2.16). These photoelectric devices are said to be used to determine a correcting value for the inclination of the material surface being conveyed on the blade via each devices respective period of light-dark time.

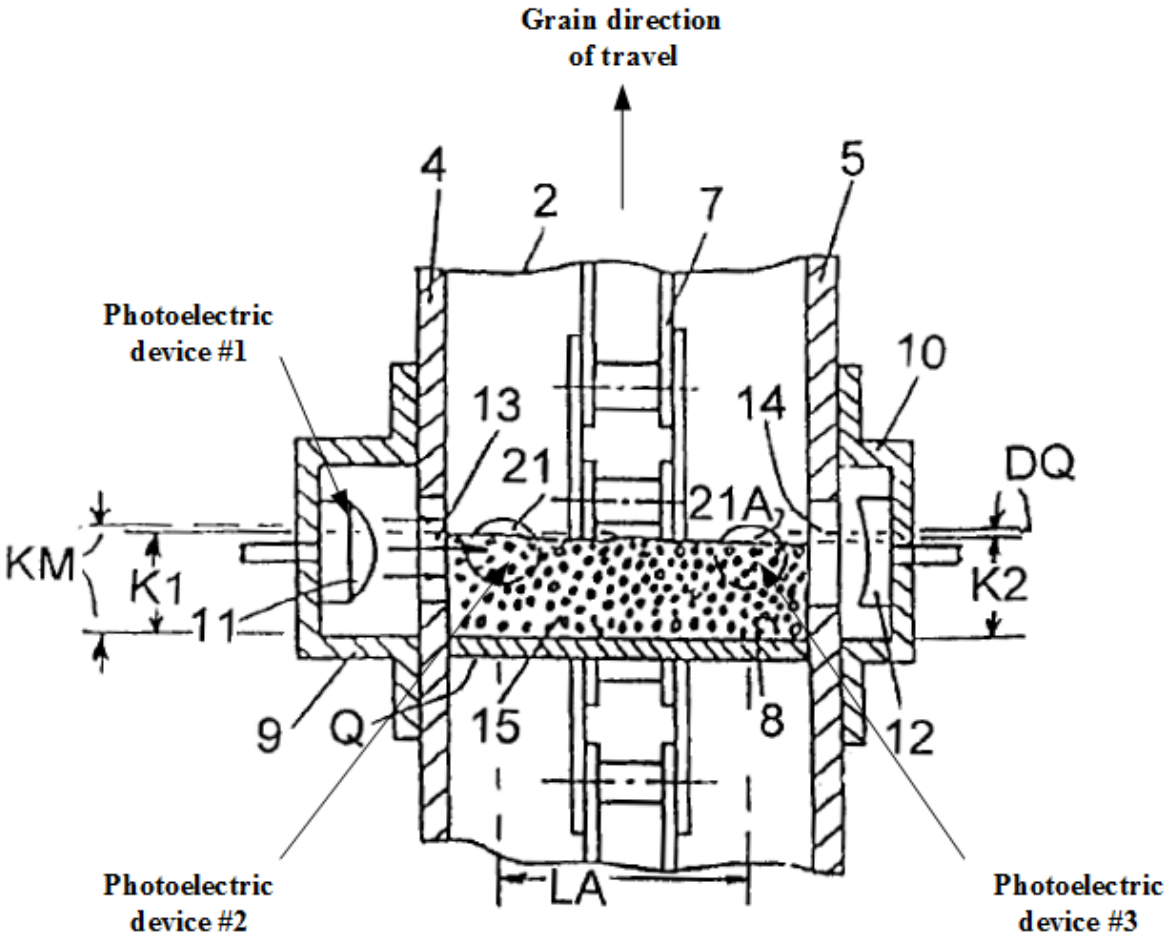


**Figure 2.16 : Photoelectric device positioning**

**Figure Credit: (U.S. Patent No. 6,282,967)**

The combination of the three photoelectric devices light-dark periods are used to calculated the average depth of the material on the blade based on orientation and position (Figure 2.17). This method is claimed to be a highly accurate method for determining the volume of material on each conveying blade.

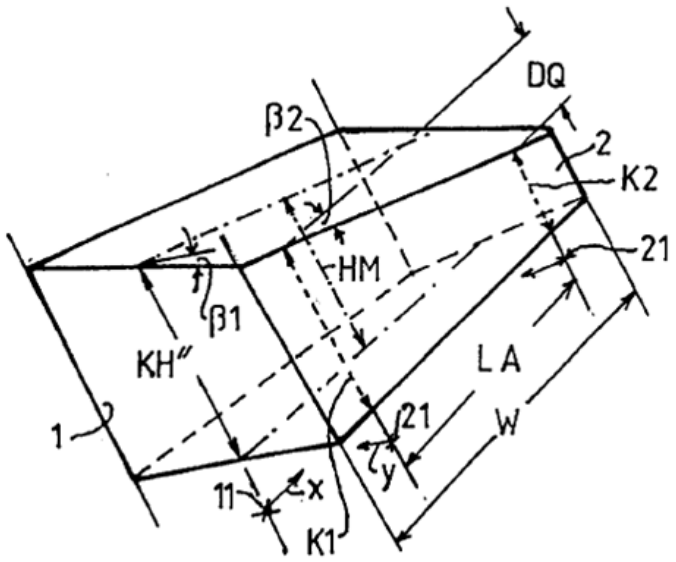


**Figure 2.17 : Estimated volume of material on individual conveyer blade**

**Figure Credit: (U.S. Patent No. 6,282,967)**

**U.S. Patent Application Publication No. US 2017/0311543 A1**

CNH Industrial patent application publication claims the novelty of using at least one optical sensor for measuring the volume of tailing passing through a tailings conveyance. The tailings conveyance, consisting of at least one rotating impeller paddle and conveyance housing, recycles tailing through a threshing and separating or cleaning system of a combine harvester. The at least one optical sensor may include an optical emitter and an optical receiver, or one sensor having the capabilities to both emit and receive a reflected light.

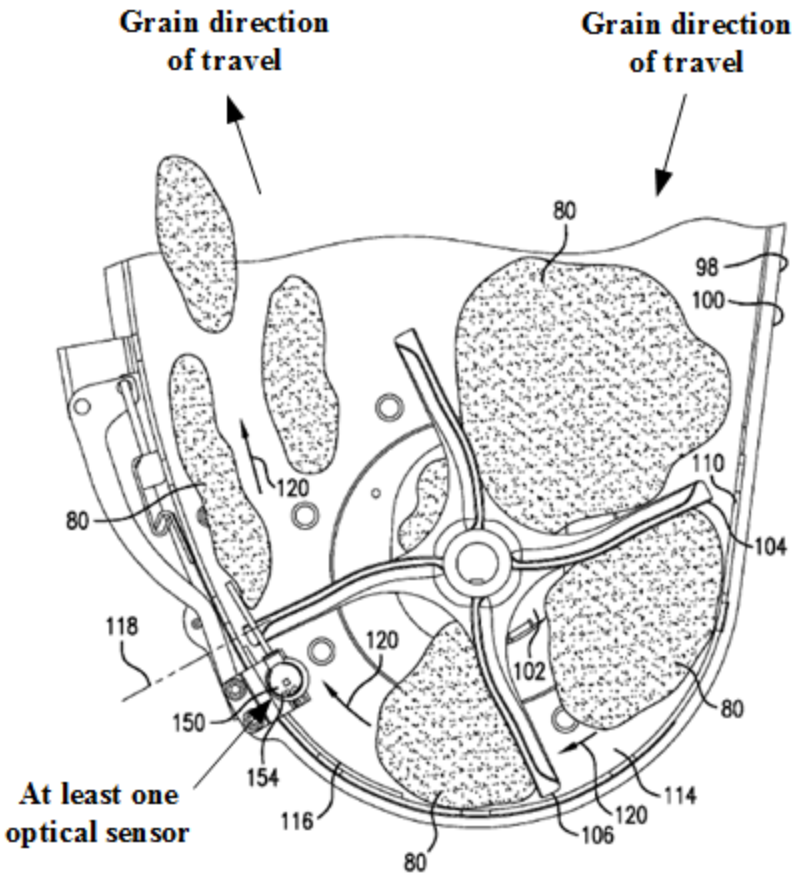


**Figure 2.18 : Optical tailings sensor in CNH tri-sweep tailing housing**

**Figure Credit: (U.S. Patent Application Pub. No. US 2017/0311543 A1)**

CNH Industrial claims that the at least one optical sensor detects the obscuration time between the optical emitter and receiver by either tailings material or protrusions of rotation elements at a high instantaneous rate. A controller element is said to determine the amount or percentage of the time that obscuration time between the optical emitter and receiver is due to the rotation element and deduct the time or percentage of only the tailing material.

CNH Industries states that the advantage of the invention is that it accurately measures the volume of tailing moving through a tailings conveyance. In additional, they claim the ability to determine the speed of the rotating element and the velocity of the tailing material.

**U.S. Patent No. 9,714,856**

Ag Leader patented the idea to automatically compensation for the effects of grain properties on mass flow sensors. They claim that crop properties including: grain moisture, grain density, kernel size, and kernel shape, and kernel fiction characteristics can affect the accuracy of the mass flow measurement. However, through their intelligent control connected to the grain mass flow sensor, they are able to determine the mass flow sensor calibration values by minimizing the variation between the baseline curve and observed curve coefficients, determine by comparing actual load masses to measured yield monitor system masses.

**U.S. Patent No. 7,702,597 B2**

George Mason Intellectual Properties was awarded a U.S Patent for the prediction of crop yield using a piecewise linear regression with a breakpoint and weather and agricultural parameters in 2010. The assignee claims the capability to predict crop yield by inputting various agricultural parameters, such as NDVI, surface data, soil moisture, and rainfall, in a developed program. The program is said to derive a prediction equation using a non-linear multivariate optimization method. George Mason Intellectual Properties claims the prediction equation includes at least one breakpoint and optimized model coefficients. They claim the invention offers an advantageous tool to attaining the crop yield by fitting a model by input parameters.

## Conclusion

Yield monitoring technologies that provide producers with crop performance information, in real-time, are available on the commercial market today. Each of those yield monitoring technologies measures the grain flow through the combine harvester via a mass flow sensor. The two most common types of mass flow sensors are impact-based and optical

beam-based. Optical beam-based mass flow sensors commonly use two opposed photoelectric sensors to measure the height of grain on a clean grain elevator paddle. Mass flow rate is obtained by multiplying the measured grain height, number of clean grain elevator paddles per second, the area of a clean grain elevator paddle, and the grain test weight. This research will focus on the application of an optical beam-based mass flow sensor and the development of a mass flow algorithm.

# CHAPTER 3. OVERVIEW OF RESEARCH OJECTIVES

The long-term goal of this research was to quantify the engineering drivers for improving the accuracy of an optical beam-based yield monitor. The short-term goal was to identify a relationship between the output response from an optical beam-based mass flow sensor and grain mass flowing through the clean grain elevator. The key research objectives for the development of an optical beam-based mass flow yield monitor algorithm included:

1. Quantify a relationship between the optical beam-based mass flow sensor output response and the corresponding grain mass produced from an individual clean grain elevator paddle.
2. Optimize and select system components in the clean grain elevator to improve the accuracy of the optical beam-based mass flow sensor.

# CHAPTER 4. OPTIMIZATION AND SELECTION OF SYSTEM COMPONENTS

## Introduction

Increasing the accuracy of the yield data, produced from a mass flow sensor, requires the optimization of the mechanical system and a robust software algorithm. The focus of this chapter was to investigate the mechanical application of an optical beam-based mass flow sensor within the clean grain elevator system and determine a methodology for the optimization and selection of system components within the clean grain elevator. The key research objectives for the optimization and selection of system components were to:

1. Evaluate and select the design of the clean grain elevator paddle.
2. Identify the optimal sensor placement and adequate sampling frequency for the output response of the optical beam-based mass flow sensor under treatment factors: grain moisture content, grain test weight, machine orientation, and clean grain elevator speed.

## Materials and Methods

### Single Paddle Test Stand

The short-term goal of this research was to identify a relationship between the output response of an optical beam-based mass flow sensor and grain mass flowing through the clean grain elevator. In order to rapidly produce the quantitative data needed to describe a relationship, a unique test stand was constructed. The test stand provided the ability to singulate the output response of the optical beam-based mass flow sensor and the corresponding mass on one individual clean grain elevator paddle.

In pursuance of singulation, the Single Paddle Test Stand (SPTS) was manufactured at Iowa State's BioCentury Research Farm. The SPTS comprised of a specially designed

clean grain elevator chain that consisted of only one clean grain elevator paddle and mounting bracket (Figure 4.1). The single paddle clean grain elevator chain is driven by a 20 HP electric motor powered from a variable frequency drive (VFD).

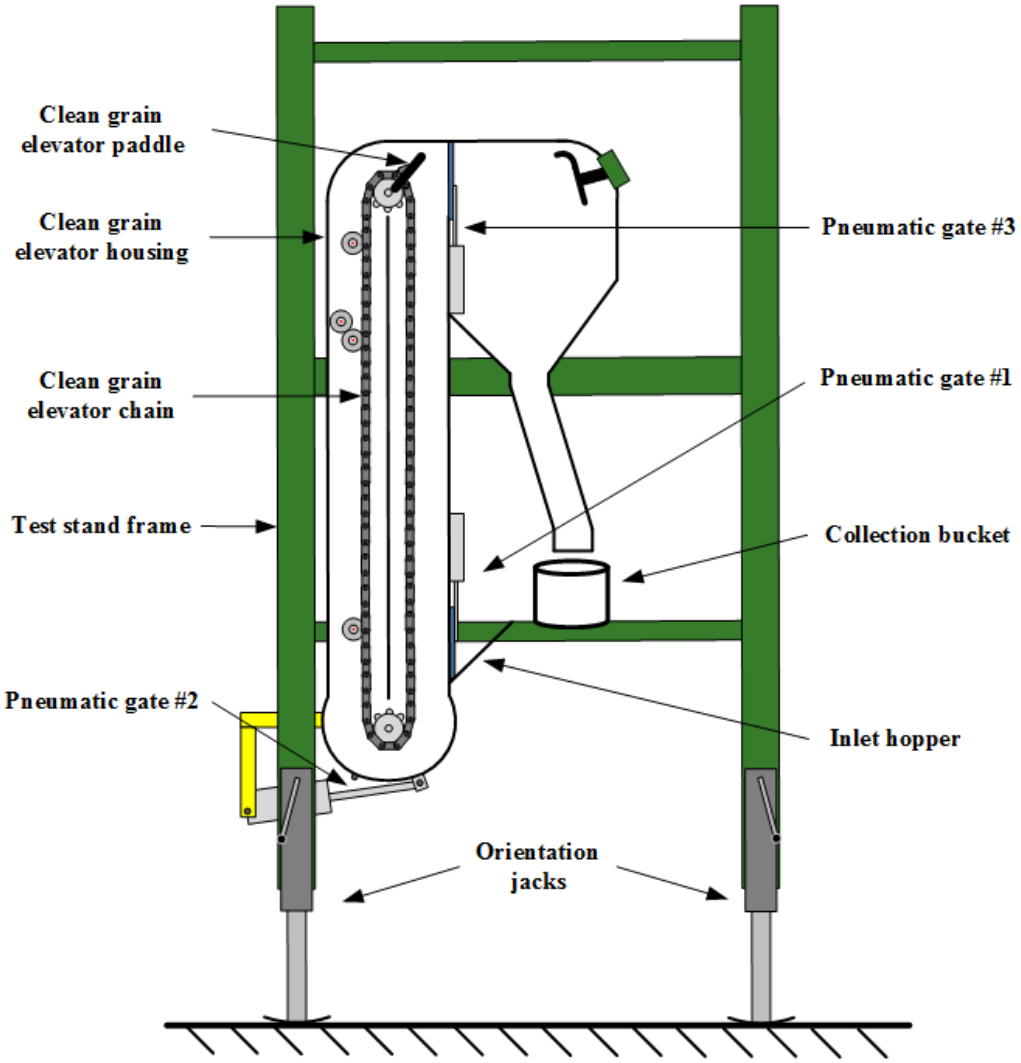


**Figure 4.1 : Single paddle test stand (SPTS)**

The SPTS clean grain elevator configuration was similar to the one found in a John Deere S670 combine harvester. In addition, the SPTS clean grain elevator configuration included an inlet hopper, three pneumatic gates, a collection chute, a tubular steel frame that encloses the entire elevator, and orientation jacks. The fountain auger and horizontal cross auger were not installed in the SPTS. Because the SPTS did not use a horizontal cross auger

to input the grain into the clean grain elevator, a cover was designed to fill the void. The cover, pressed fitted onto the lower shaft of the clean grain elevator, rotated with the clean grain elevator and prevented the grain from flowing into the cross auger cavity. It was assumed that the cover did not affect the measurement of the optical beam-based mass flow sensor.

The three pneumatic gates on the SPTS were used to control the flow of grain through the clean grain elevator. Pneumatic gate #1, located in the inlet hopper on the front side of the stand, controlled the inflow of grain in the stand. The second pneumatic gate, installed on the bottom of the clean grain elevator housing, dumped any grain the clean grain elevator paddle did not discharge into the collection chute. The last pneumatic gate, pneumatic gate #3, controlled the singulation of grain from the clean grain elevator paddle by opening before and closing after the grain was discharged from the clean grain elevator paddle.

**Data acquisition system**

The data acquisition system used on the SPTS was a National Instruments (NI) cRIO-9038 with 8 module slots in the chassis (Figure 4.2). NI modules 9403, 9234, 9205, and 9853 were used for the collection of various digital, high frequency, analog, and CAN signals, respectively. Because a VFD was used to drive the electric motor, the tubular frame of the SPTS and instrumentation were deliberately grounded using a grounding stake to reduce the introduced baseline noise in the instrumentation output signals caused by the VFD.


**Figure 4.2 : NI cRIO with modules**

**Optical beam-based mass flow sensor positioning**

Four optical beam-based mass flow sensors were used in the evaluation of the optimal positioning of the mass flow sensor (Figure 4.3). Beams I, II, IV were aligned all in the same vertical plane approximately 64 mm from the rear housing of the clean grain elevator. Beam III was vertically aligned approximately 50 mm from the rear housing of the clean grain elevator, 14 mm closer than Beams II and IV. Beam I was positioned approximately 610 mm above the lower shaft of the clean grain elevator. Beams II and III were positioned about 1924 mm and 1988 mm above the lower shaft, respectively. Beam IV was positioned nearly at top of the clean grain elevator, 203 mm below the upper shaft. At the height location of Beam IV, a rotating drive pulley on the inner side of the clean grain elevator required a smaller body model of photoelectric sensor than what was used for Beams I, II, and III (Table 4.1).

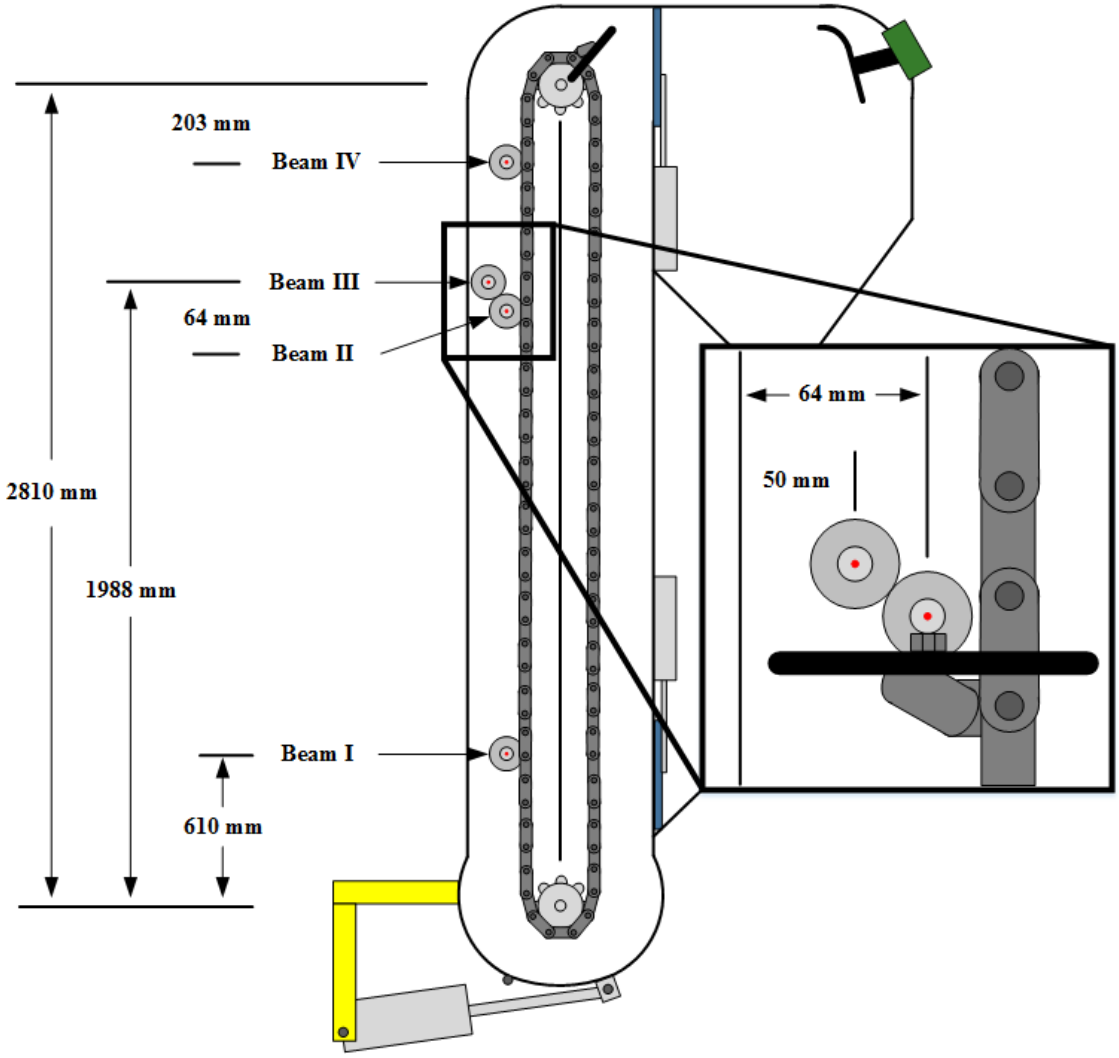


**Figure 4.3 : SPTS optical beam-based sensor positioning and nomenclature**

**Table 4.1 : Optical beam-based sensor manufacturer information**

| Component nomenclature | Sensor manufacturer | Part number | |
|---|---|---|---|
| | | Emitter | Receiver |
| Beam I | Raven Industries | 063-9000-006 | |
| Beam II | Raven Industries | 063-9000-006 | |
| Beam III | Raven Industries | 063-9000-006 | |
| Beam IV | Banner Engineering | 61618 | 61624 |

**SPTS operation**

Controlling the grain flow through the clean grain elevator of the SPTS, the SPTS operation, was done using a LabVIEW program that interactively linked with the NI cRIO via Ethernet. The LabVIEW program controlled various functions during the SPTS operation, including: driving electronic valves attached to the pneumatic gates, starting and stopping data collection, incrementing repetition numbers, and writing summarized binary files. The SPTS operation encompassed five major states.

The first state in the SPTS operation, STATE 1, was initiated by starting the LabVIEW program. In STATE 1, a grain sample was loaded into the inlet hopper of an already rotating clean grain elevator. All three pneumatic gates were forced closed in STATE 1. The SPTS operation remained in STATE 1 until two triggers occurred. The first trigger was the Run Sample button on the LabVIEW program user interface had be pressed. After the Run Sample button was pressed, Beam I had to record a blockage, identifying the location of the clean grain elevator paddle.

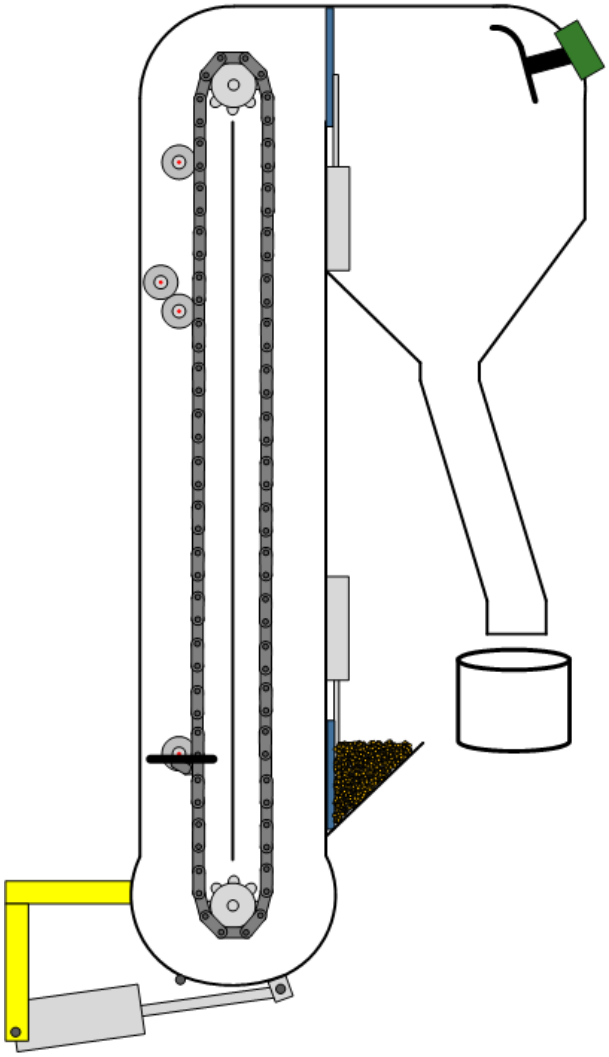

**Figure 4.4 : SPTS STATE 1**

After the two triggers in STATE 1 were satisfied, the SPTS operation moved into STATE 2. In STATE 2, Pneumatic gate #1 was forced open, allowing gravity to let the loaded grain sample fall into the bottom of the clean grain elevator. Pneumatic gates #2 and #3 remained closed and the clean grain elevator paddle continued to rotate toward the newly inlet grain. The SPTS operation remained in this state until the clean grain elevator paddle was located just above Pneumatic gate #1. The LabVIEW program then forced Pneumatic gate #1 closed and moved into STATE 3.

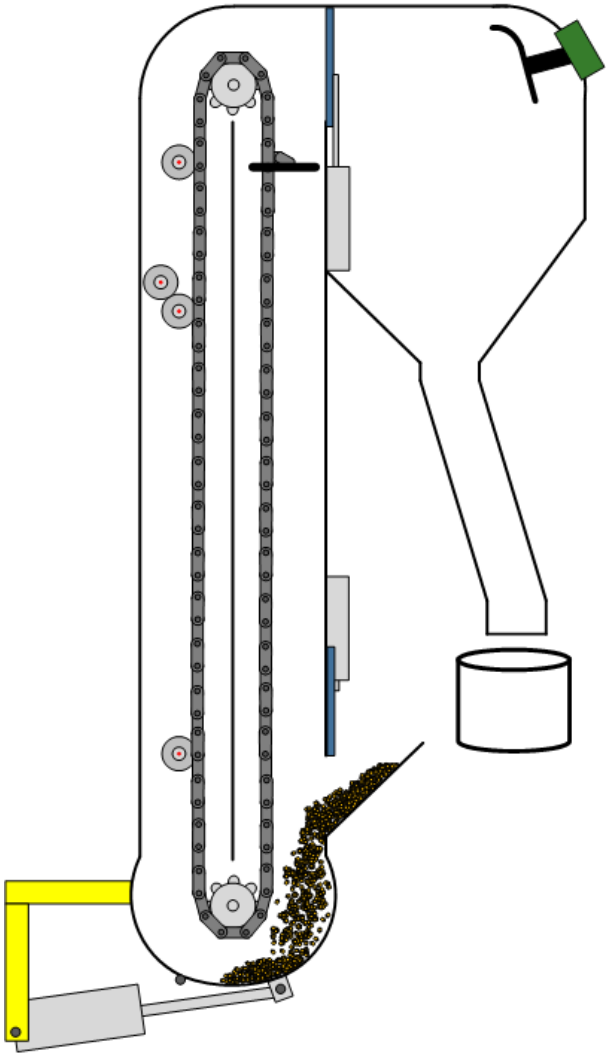

**Figure 4.5 SPTS STATE 2**

In the third state in the SPTS operation, the grain sample was carried up the clean grain elevator by the clean grain elevator paddle causing each of the four optical beam-based mass flow sensors to output a distinct blocked response. Because all the grain sample was not carried up the clean grain elevator by the clean grain elevator paddle, Pneumatic gate #2 was triggered open to allow the remaining or falling grain to exit out the bottom of the clean grain elevator. While the clean grain elevator paddle ascended up the clean grain elevator, Pneumatic gate #3 was forced open to allow the grain sample to be discharged into the collection chute.

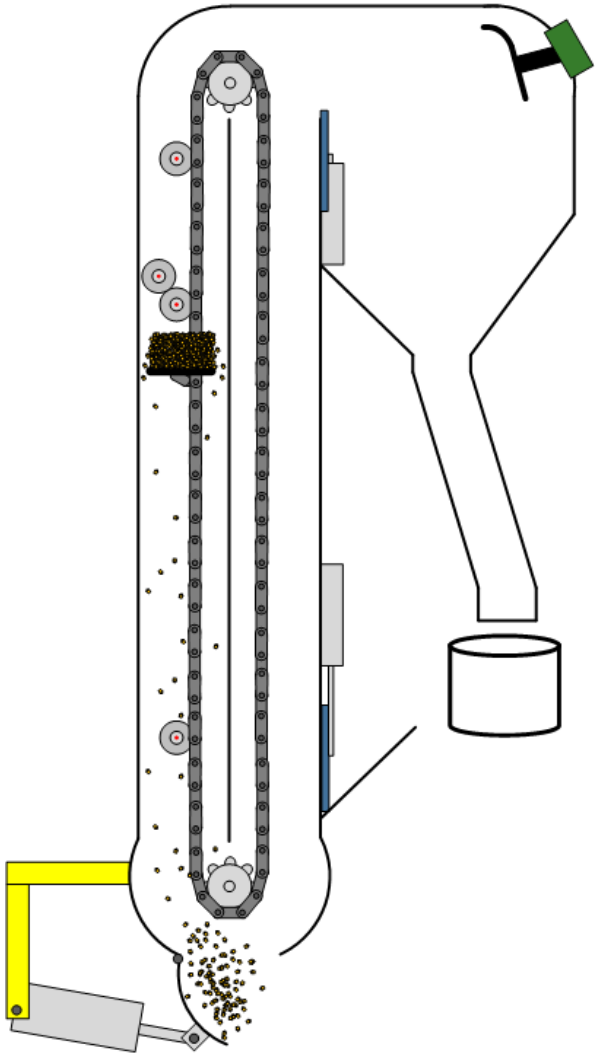

**Figure 4.6 : SPTS STATE 3**

After the grain was discharged from the clean grain elevator paddle, the clean grain elevator paddle rotated downward, forcing any resting grain on the paddle out the bottom of the clean grain elevator. Pneumatic gate #3 was then forced closed again to singulate the discharged grain from any additional grain due to continuing rotating clean grain elevator.

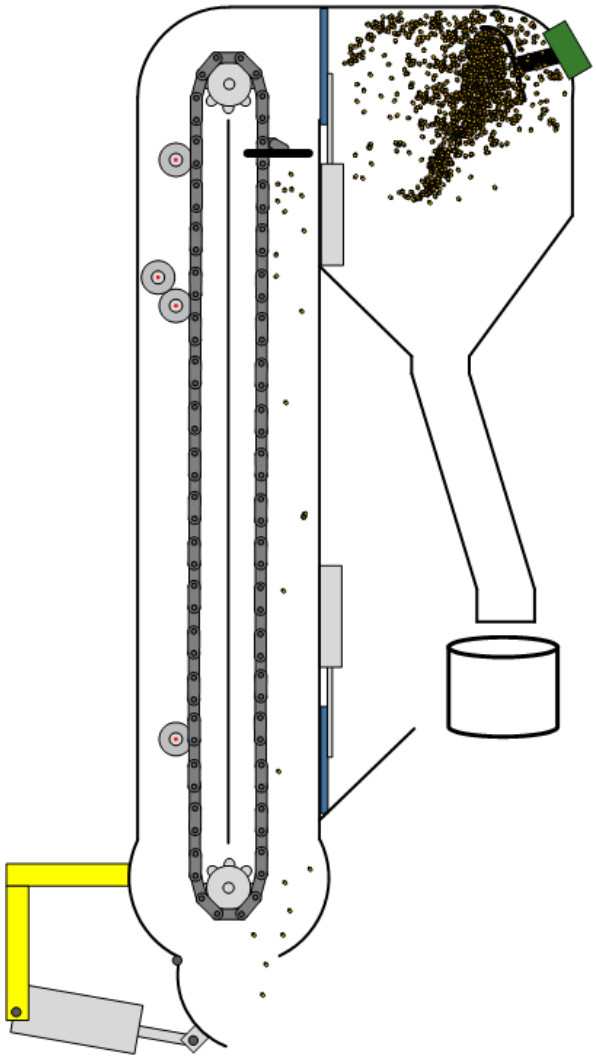

**Figure 4.7 : SPTS STATE 4**

The final state in the SPTS operation was STATE 5. In this state, all the pneumatic gates were forced closed and the discharged grain sample fell down the collection chute into the collection bucket. The collection bucket was weighed and the corresponding mass was recorded to later be examined against the optical beam-based mass flow sensors output blockages. The scale used for the weighing of the collection bucket and the grain sample was a VWR portable scale. It was calibrated using certified scale weights, ranging from 100 to 5,000 grams. The accuracy of the calibration was confirmed before each test was conducted

by placing the same scale weights on the scale and verifying that the output error was less than 1%.

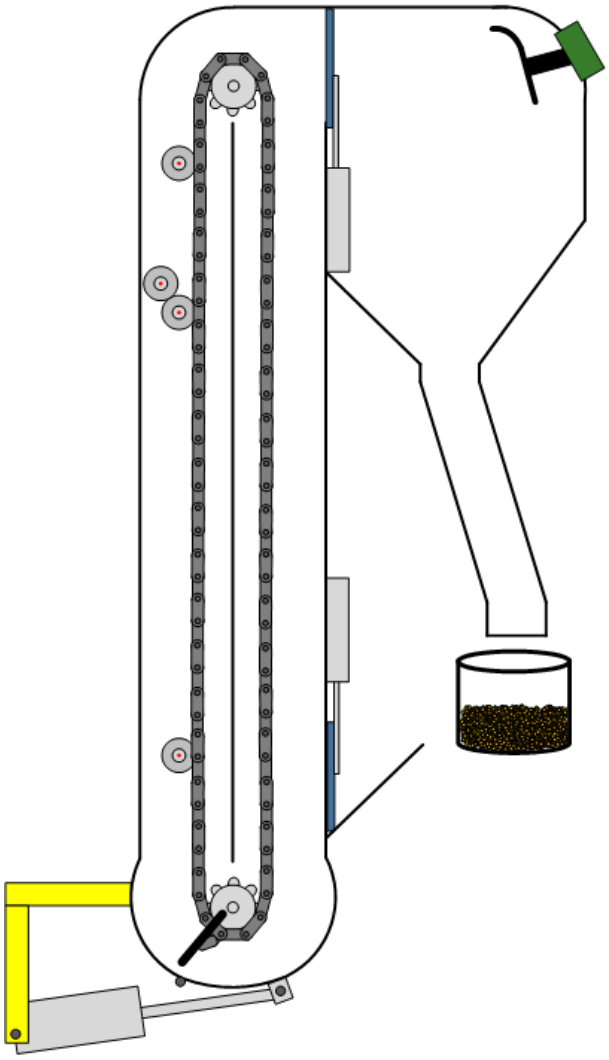

**Figure 4.8 : SPTS STATE 5**

**Clean Grain Elevator Paddle Design Optimization**

As discussed prior, optimization of the clean grain elevator components is an essential part in improving the accuracy of yield data. Four design concepts of the clean grain elevator paddle were considered in the development of the optimized system (Figure 4.9).

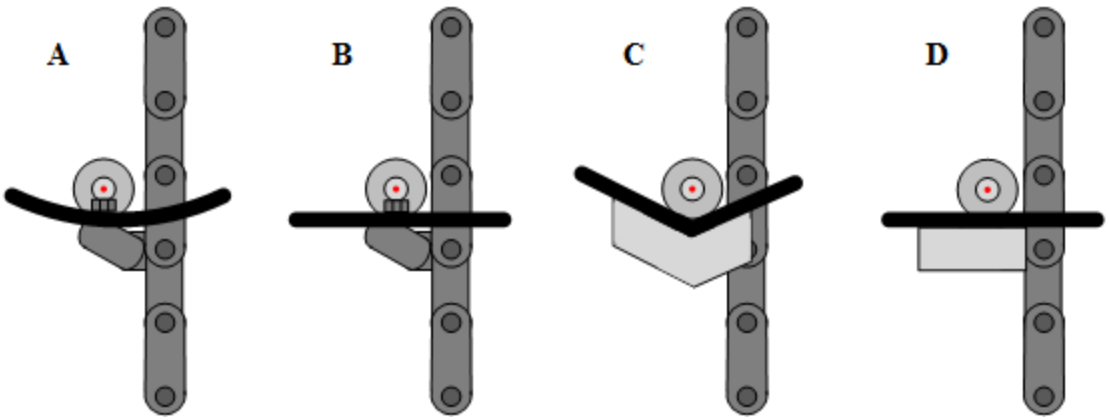


**Figure 4.9 : Clean grain elevator paddle design concepts**

**A: Concept #1 (John Deere); B: Concept #2 (May Wes); C: Concept #3; D: Concept #4**

John Deere's current production clean grain elevator paddle, Concept #1, consists of a rubber paddle that is manufactured from recycled tire carcasses. The advantages this design concept has is that it has low interactive wear between the clean grain elevator paddle itself and the clean grain elevator housing and it is already in production. The disadvantages of this design is that each clean grain elevator paddle can have a different shape, thickness, and stiffness. Additionally, the bolt heads and mounting bracket can add variability into the measurement.

Concept #2, the May Wes design, provides more consistency from clean grain elevator paddle to clean grain elevator paddle than that of Concept #1. Concept #2 features a manufactured, rigid, high-density plastic paddle that is flat rather than cupped. This flat paddle shape additionally reduces variability in the measurement but still includes bolt heads and the mounting bracket in the measurement. For example, the variability that just the mounting bracket design can introduce on the tare value can add or subtract approximately half of a millimeter in height for every millimeter in lateral movement.

The focus of the design in Concept #3 was to combine the designs of both Concept #1 and Concept #2, while eliminating the bolt heads and mounting bracket from the

measurement. In this clean grain elevator paddle design, an inset occurs where the bolt heads fasten to the mounting bracket, covering them from the measurement. Additionally, in Concept #3, the clean grain elevator paddle design channels the grain pile on the clean grain elevator paddle toward the measurement. This increases the amount of material at the measurement, which could help with accuracy at low grain flow rates. This design also improved clean grain elevator paddle to clean grain elevator paddle consistency, similar to Concept #2, by using a rigid, high-density plastic. Lastly, a mounting bracket shield was also included in the design to match the geometry of the clean grain elevator paddle design to aid in tare value consistency. The two major disadvantages that Concept #3 has are that at low clean grain elevator chain tension, even with the mounting bracket shield, lateral movement can still induce high accuracy errors and that the cupped geometry introduces nonlinearity into the filling of the clean grain elevator paddle.

Concept #4, highlights the benefits of both Concept #2 and Concept #3. It consists of a modified May Wes rigid, high density plastic clean grain elevator paddle with inset bolt heads and a mounting bracket shield. The major difference between Concept #4 and Concept #3 are that despite lateral movements in the clean grain elevator paddle during the measurement, the tare value remains consistent. Additionally, the clean grain elevator paddle geometry does not induce nonlinearity while filling. The disadvantage that Concept #4 has, and all the other concepts, is at extremely low clean grain elevator chain tension the rotation of the clean grain elevator paddle can still cause high accuracy errors.

The selection of the design concept to move forward with for future development was determined using a decision matrix (Table 4.2). The results of that decision matrix concluded that Concept #4 ranked the highest upon the four concepts for the given criteria. The final

design of Concept #4 included six parts: two countersunk bolts, two locking nuts, one mounting bracket shield, and one modified May Wes clean grain elevator paddle.

**Table 4.2 : Clean grain elevator paddle design decision matrix**

| Selection criteria | Clean grain elevator paddle design | | | |
|---|---|---|---|---|
| | Concept #1 | Concept #2 | Concept #3 | Concept #4 |
| Production part | 1 | 0 | 0 | 0 |
| Inset bolt heads | 0 | 0 | 1 | 1 |
| Mounting bracket shield | 0 | 0 | 1 | 1 |
| Paddle to paddle consistency | 0 | 1 | 1 | 1 |
| Tare value consistency | 0 | 0 | 0 | 1 |
| Linear filling | 0 | 1 | 0 | 1 |
| Net score | 1 | 2 | 3 | 5 |
| Rank | 4 | 3 | 2 | 1 |

## Experimental Factors

### Crop properties treatments

Grain moisture content was noted by McNaull, in 2016, to have a statistically significant effect on the performance of impact-based mass flow sensors. In that study, when grain moisture content exceeded 22.5%, the mean error experienced was greater than 7.5%. Although the optical beam-based mass flow sensor is not an impact-based sensing technology, grain moisture content was selected as a treatment factor to study the effects that it has on the pile of grain on the clean grain elevator paddle. In this study, the grain moisture content treatment levels were 14%, 25%, and 30%. The desired higher moisture content treatment levels were achieved by wetting the grain from the lowest treatment level, 14%, to the desired higher moisture content in a sealed rotating drum for over 48 hours. Physical inspection of the samples after 48 hours confirmed that the entire grain sample had adsorbed

all the added water and was at the same equilibrium moisture content. The final moisture content was confirmed using a GAC 2500 grain properties analyzer.

Grain test weight, as discussed prior, is unmeasured on current combine harvesters, but since it is needed to relate the volumetric measure of the optical beam-based mass flow sensor to actual mass flow rate, it was selected to be studied as a treatment factor. The grain test weight treatment factor consisted of three treatment levels: 55 lb/bu, 58 lb/bu, and 59 lb/bu. In an attempt to decouple the inverse relationship between grain moisture content and test weight, the treatment levels in the grain test weight treatment factor were achieved by adding material to a clean grain sample. The 55 lb/bu and 59 lb/bu treatment levels were the result of adding 10% broken corn cob and 10% broken corn kernels to each of the grain samples total weights, respectively. The samples were mixed thoroughly prior to testing to ensure that the entire grain sample contained an even distribution of the 10% additive material.

**Mechanical treatments**

Prior literature states that machine orientation has a statistically significant effect on the performance of optical beam-based mass flow sensors. It was selected as a treatment factor with five treatment levels. In 2016, Schuster evaluated the effect a combine harvester's pitch angle and roll angles, up to 3 degrees, had on yield monitor performance. This study evaluated a combine harvester pitch angle and roll angle up to 5 degrees. The pitch and roll angles of a combine harvester were mimicked on the SPTS by varying the height of the orientation jacks attached to the SPTS's tubular framed. The angle of inclination of the clean grain elevator was verified using a Westward electronic protractor. It was properly calibrated before each treatment level testing and the measurements were taken from the same spot on

the clean grain elevator. The positive direction of pitch and roll angles were noted as pitch ahead and roll to the right (Figure 4.10).

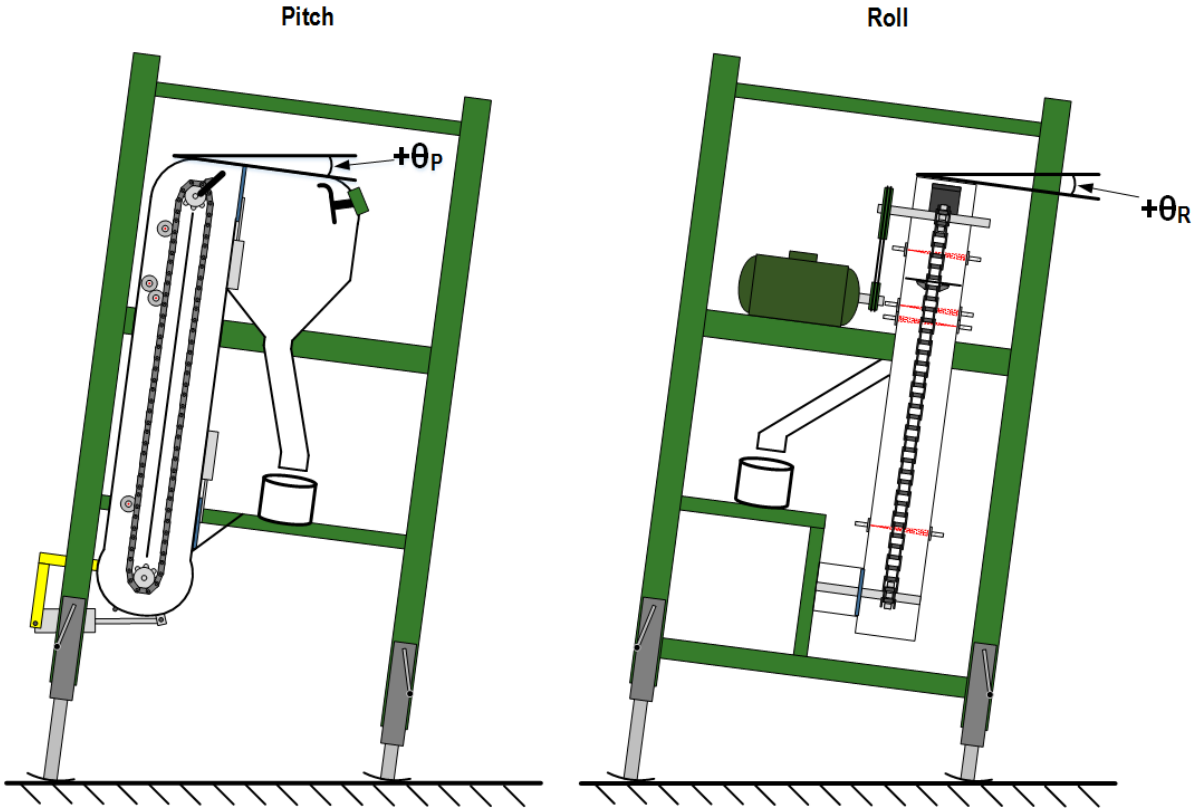


**Figure 4.10 : SPTS positive machine orientation angles**

Because clean grain elevator speed is directly used to relate the output blockage time back to the actual height of grain on the clean grain elevator paddle, it was selected as a treatment factor with treatment levels from 400 to 500 rpm. The normal operating speed of a John Deere S670 is approximately 420 rpm. On the SPTS, the speed of the clean grain elevator was dictated by varying the frequency of the VFD powering the electric drive motor mounted the SPTS.

**Grain mass flow rate treatment level**

The grain mass flow rate was determined to be a secondary treatment level under each of the crop properties and mechanical treatment levels. The treatment levels of the grain

mass flow rate treatment level were determined using the normal distributions of grain flow rate (McNaull, Figure 4.11). The normal distributions of the grain mass flow rate were produced using the output from current impact-based mass flow sensor, observed over thousands of loads.

**Figure 4.11 : Normal distribution of grain flow rate**

**Figure Credit: (McNaull, 2016)**

The observed standard deviation of the normal distribution for corn mass flow rate was nearly three times the observed standard deviation of wheat, soybeans, and canola. Because of corn's large dynamic operating range, it was the only crop selected for experimental design. The targeted treatment levels were determined to be plus and minus one and two standard deviations ($\sigma$) from the mean ($\mu$) grain mass flow rate (Table 4.3). The target mass flow rate was dictated during test stand operation by varying the input mass into the SPTS.

**Table 4.3 : Grain mass flow rate treatment levels**

| Normal distribution | Treatment level: targeted mass flow rate (kg/s) |
|---|---|
| -2σ | 1 |
| -σ | 7 |
| μ | 13 |
| σ | 20 |
| 2σ | 27 |

**Experimental Design**

The goal of experimental design for the identification of the optimal sensor placement and adequate sampling frequency for the output response of the optical beam-based mass flow sensor was to minimize any experimental bias. To minimize experimental bias, a control data set was established where the crop properties were not manipulated and mechanical treatment factors were set at normal combine harvesting conditions. The control, crop properties, and mechanical treatment factors utilized a randomized block design, where each treatment factor of a homogeneous grain sample was evaluated across randomly selected grain mass flow rate treatment levels (Table 4.4). The randomization of grain mass flow rate treatment levels was determined using a random number generator. Each data set produced consisted of approximately 75 or more randomly selected grain mass flow rate treatment levels.

A full factorial experimental design was not utilized for the experimentation due to time and resource constraints. A full factorial experimental design for the selected treatment factors and number of levels would consist of over 240 total data sets and over 18,000 total mass flow rate treatment levels. The experimental design used focused on the manipulation

of only one treatment factor per data set. The limitation of the experimental design was it did not consist of any interactive total data sets.

**Table 4.4 : Experimental design**

| Data set | Treatment Factor | Treatment level #1 | | | | | Treatment level #2 |
|---|---|---|---|---|---|---|---|
| | | Grain moisture content (%) | Grain test weight (lb/bu) | Clean grain elevator speed (rpm) | Pitch angle (°) | Roll angle (°) | Grain mass flow rate (kg/s) |
| A | Control | 14.2 | 58.7 | 420 | 0 | 0 | 1-27 |
| B | Grain moisture content | 24.6 | 51.5 | 420 | 0 | 0 | 1-27 |
| C | Grain moisture content | 30.4 | 50.6 | 420 | 0 | 0 | 1-27 |
| D | Grain test weight | 14.3 | 55.1 | 420 | 0 | 0 | 1-27 |
| E | Grain test weight | 13.8 | 59.1 | 420 | 0 | 0 | 1-27 |
| F | Clean grain elevator speed | 14.2 | 58.7 | 400 | 0 | 0 | 1-27 |
| G | Clean grain elevator speed | 14.2 | 58.7 | 500 | 0 | 0 | 1-27 |
| H | Machine Orientation | 14.2 | 58.7 | 420 | 5 | 0 | 1-27 |
| I | Machine Orientation | 14.2 | 58.7 | 420 | -5 | 0 | 1-27 |
| J | Machine Orientation | 14.2 | 58.7 | 420 | 0 | 5 | 1-27 |
| K | Machine Orientation | 14.2 | 58.7 | 420 | 0 | -5 | 1-27 |

**Methodology for Evaluation of Performance**

The output signals from each of the four optical beam-based mass flow sensors were recorded by the NI cRIO-9038 attached to the SPTS. Each optical beam-based mass flow sensor's output signal was logged at 2,000 Hz frequency. Additionally, the output signals from Beams II and IV were also simultaneously recorded at 10,000 Hz frequency. The nomenclature used to describe those two responses was Beam II_HFQ and Beam IV_HFQ.

Once a data set's testing was complete, the binary data files written to the NI cRIO-9038 were downloaded and processed using MATLAB. The output signals for each sensor were also processed using a MATLAB function to convert the raw voltage signal to a filtered binary signal. The filtered binary signal corresponded a zero as an unblocked light beam and denoted a one for interrupted (Figure 4.12). The interruption, or pulse width, of the filtered binary signal was then analyzed to find the tare value and characteristic pulse width for each grain mass flow rate treatment level.

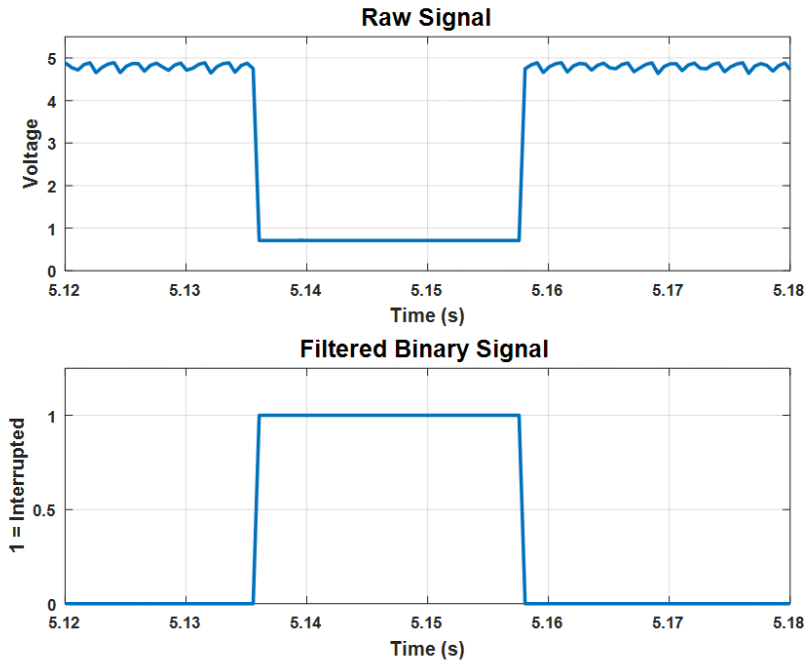


**Figure 4.12 : Voltage to binary signal filtering**

Because the clean grain elevator was continuously rotating during the testing for each data set, the first pulse width, when the clean grain elevator paddle was completely empty, was determined to be the grain mass flow rate treatment level tare value pulse width. The characteristic pulse width, or pulse width when the loaded grain sample riding on the clean grain elevator paddle caused the interruption, was determined using the know state in the SPTS operation and secondary sensors. The tare value and characteristic pulse widths were then related back to height measurements through the clean grain elevator speed, clean grain elevator sprocket information, and sampling frequency (Equation 4.1).

**Equation 4.1 : Height measurement estimation**

$$Height\ (mm) = Pulse\ width\ (indices) * Sampling\ frequency^{-1}\ \left(\frac{sec}{indices}\right) * Clean\ grain\ elevator\ speed\left(\frac{rev}{\min}\right) * Sprocket\ infomation\left(\frac{teeth}{rev}\right)\left(\frac{mm}{tooth}\right) * \left(\frac{min}{60\ \sec}\right)$$

The measured tare value height for each grain mass flow rate treatment level in a data set was compiled and analyzed to evaluate the spread in that measurement. The characteristic height measurement was compared to the corresponding mass recorded for each grain mass flow rate treatment level. A linear curve fit was then applied to the accumulation of the characteristic height measurements and recorded grain masses for each independent data set. The linear curve fit was done using a MATLAB curve fitting tool.

In order to determine the adequate sampling frequency and optimal sensor placement for the optical beam-based mass flow sensor, four performance statistics were used:

1. Tare value standard deviation – $\sigma_{tare}$
2. Coefficient of determination – $R^2$
3. Sum of squares due to error – SSE
4. Root mean square error – RMSE

## Results and Discussion

### Performance Impact of Sensor Position

#### Beam I location

Early evaluation of experimental control, data set A, the relationship between the height measurements of Beam I and the recorded masses demonstrated that the location of Beam I experienced considerably higher variability compared to the other three locations (Figure 4.13). For the same data set, the coefficient of determination for Beam I was nearly 40% lower than each of the other three locations. The increased variability at the Beam I location was determined to be the result of the settling time that the grain had experienced on the clean grain elevator paddle before the measurement took place. This variability was determined to be significant enough to remove the Beam I location from future consideration.

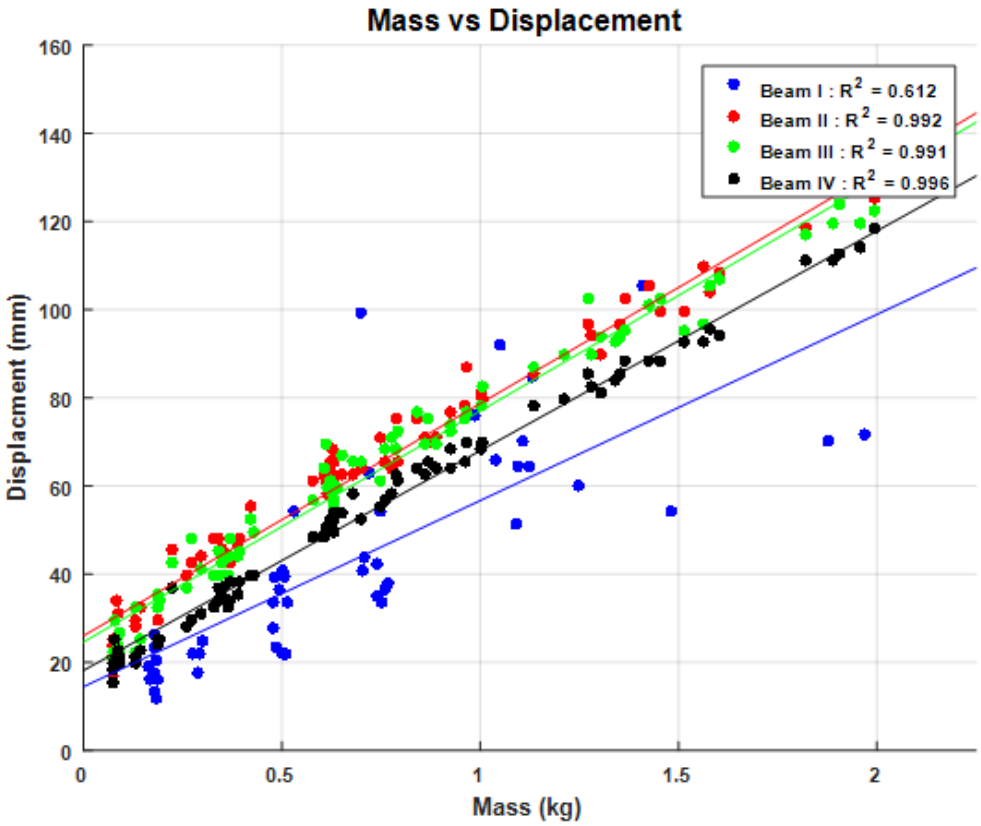


**Figure 4.13 : All beams mass vs displacement**

**Tare value consistency**

The ability to consistently present the same tare value measurement to the optical beam-based mass flow sensor was determined to be pivotal to the system's performance. The standard deviation of the tare value was evaluated at each sensor location to analyze the consistency of tare value measurement. The results from over 160 randomly selected tare value measurements for each sensor location concluded that the standard deviation for each sensor location was under 1 mm (Table 4.5). For comparison, multiplying the standard deviation with the standard test weight of corn, the average rate of clean grain elevator paddles in a John Deere S670 combine harvester clean grain elevator, and clean grain elevator paddle area; the equivalent mass flow rate for each standard deviation was less than

the 1st percentile in the normal distribution for corn mass flow rates. Based on the standard deviation of tare value measurement for each sensor location, it was determined that each sensor location was adequate for further analysis.

**Table 4.5 : Statistical comparison of the tare value by sensor position**

| Sensor | $\sigma_{tare}$ (mm) | Equivalent mass flow rate (kg/s) | Mean (mm) | Median (mm) | Standard Error (mm) |
|---|---|---|---|---|---|
| Beam II | 0.70 | 0.18 | 45.09 | 44.65 | 0.055 |
| Beam III | 0.84 | 0.22 | 45.41 | 46.09 | 0.066 |
| Beam IV | 0.66 | 0.17 | 41.33 | 41.77 | 0.052 |

An additional analysis was performed to verify the quality of the tare value data. The mean and median for each sensor location was calculated and compared against the actual physical height of the clean grain elevator paddle used during testing. The actual physical height of the clean grain elevator paddle was measured at 48.88 mm, using calipers. When compared against both the mean and median at each sensor location, the measured tare values were notably smaller. This confirms the observed height measurement from a photoelectric sensor was less than the actual physical height due to the beam pattern from the photoelectric emitter.

Lastly, an investigation into the measurement uncertainty in the tare value for each of the optical beam-based mass flow sensors was conducted to understand the dispersion in their measurements. The two measurement uncertainty parameters used were repeatability and quantization error. Repeatability was determined using the standard error (SE). Quantization error was determined by analyzing the distance between the sampling frequency indices (Figure 4.14). The results from the measurement uncertainty investigation exhibited that the tare values for Beams II, III, and IV have a standard uncertainty of 0.056

mm, 0.067 mm, and 0.053 mm, respectively, at approximately a 68% confidence level (Table 4.6).

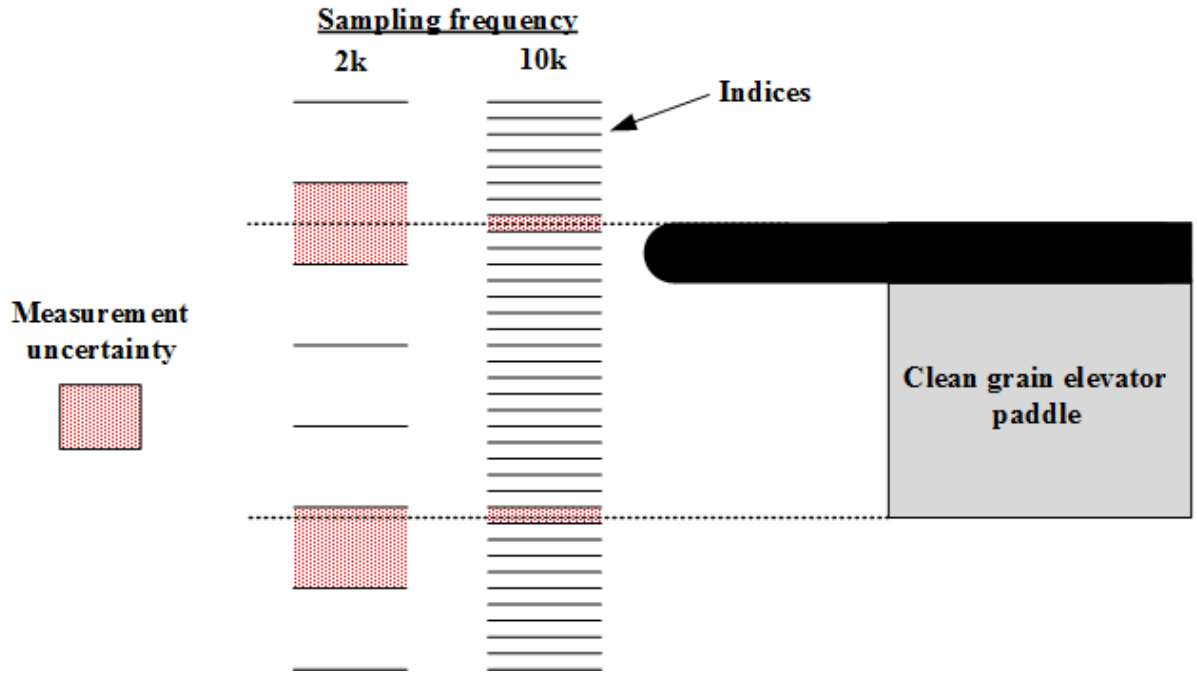


**Figure 4.14 : Quantization error due to sampling frequency**

**Table 4.6 : Tare value measurement uncertainty by sensor location**

| Sensor | Parameter | Source | Type | $u_{absolute}$ (mm) | Probability distribution, divisor | Standard uncertainty (mm) |
|---|---|---|---|---|---|---|
| Beam II | Repeatability | SE | A | 0.055 | Normal, 1 | 0.055 |
| | Quantization Error | Sampling frequency | B | 0.017 | Rectangular, $\sqrt{3}$ | 0.0098 |
| | | | | Standard | Normal | 0.056 |
| Beam III | Repeatability | SE | A | 0.066 | Normal, 1 | 0.066 |
| | Quantization Error | Sampling frequency | B | 0.017 | Rectangular, $\sqrt{3}$ | 0.0098 |
| | | | | Standard | Normal | 0.067 |
| Beam IV | Repeatability | SE | A | 0.052 | Normal, 1 | 0.052 |
| | Quantization Error | Sampling frequency | B | 0.017 | Rectangular, $\sqrt{3}$ | 0.0098 |
| | | | | Standard | Normal | 0.053 |

**Treatment factors**

The analysis of the sum of squares due to error and the root mean squared error focused on the variance between the predicted values from the linear curve fit and the actual observed values. The linear curve fit for each independent data set was evaluated using the sum of squares due to error and root mean squared error. The sensor location that exhibited the lowest variance across all treatment factors would be selected to build an optical beam-based mass flow algorithm.

**Equation 4.2 : Sum of squares due to error**

$$SSE = \sum_{i=0}^{n} (y_i - \hat{y}_i)^2$$

**Equation 4.3 : Root mean square error**

$$RMSE = \sqrt{\frac{1}{n} \sum_{i=0}^{n} (y_i - \hat{y}_i)^2}$$

**Table 4.7 : Statistical comparison of treatment factor by sensor location**

| Data set | Treatment Factor | Sensor | n-1 | $R^2$ | SSE ($mm^2$) | RMSE (mm) |
|---|---|---|---|---|---|---|
| A | Control | Beam II | 92 | 0.99 | 1667.95 | 4.26 |
| | | Beam III | 93 | 0.99 | 1921.20 | 4.55 |
| | | Beam IV | 93 | 1.00 | 684.28 | 2.71 |
| B | Grain moisture content | Beam II | 62 | 0.99 | 1705.64 | 5.25 |
| | | Beam III | 64 | 0.99 | 1591.15 | 4.99 |
| | | Beam IV | 65 | 0.99 | 1163.60 | 4.23 |
| C | Grain moisture content | Beam II | 77 | 0.99 | 2166.73 | 5.30 |
| | | Beam III | 78 | 0.99 | 2412.64 | 5.56 |
| | | Beam IV | 78 | 1.00 | 768.94 | 3.14 |
| D | Grain test weight | Beam II | 71 | 0.98 | 4163.53 | 7.66 |
| | | Beam III | 71 | 0.96 | 5778.94 | 9.02 |
| | | Beam IV | 71 | 0.98 | 3614.16 | 7.13 |
| E | Grain test weight | Beam II | 60 | 0.99 | 1223.33 | 4.52 |
| | | Beam III | 60 | 0.99 | 1089.70 | 4.26 |
| | | Beam IV | 60 | 1.00 | 438.58 | 2.70 |
| F | Clean grain elevator speed | Beam II | 65 | 0.99 | 1219.70 | 4.33 |
| | | Beam III | 65 | 0.99 | 1352.29 | 4.56 |
| | | Beam IV | 65 | 1.00 | 311.31 | 2.19 |
| G | Clean grain elevator speed | Beam II | 74 | 0.99 | 1980.82 | 5.17 |
| | | Beam III | 74 | 0.95 | 7199.76 | 9.86 |
| | | Beam IV | 74 | 0.99 | 1072.35 | 3.81 |
| H | Machine Orientation | Beam II | 71 | 0.97 | 4138.55 | 7.63 |
| | | Beam III | 71 | 0.95 | 7745.75 | 10.44 |
| | | Beam IV | 73 | 0.99 | 1906.21 | 5.11 |
| I | Machine Orientation | Beam II | 66 | 0.99 | 1740.52 | 5.14 |
| | | Beam III | 66 | 0.98 | 2512.19 | 6.17 |
| | | Beam IV | 66 | 1.00 | 459.39 | 2.64 |
| J | Machine Orientation | Beam II | 71 | 0.98 | 2957.90 | 6.60 |
| | | Beam III | 71 | 0.98 | 2928.25 | 6.56 |
| | | Beam IV | 72 | 0.99 | 1386.25 | 4.52 |
| K | Machine Orientation | Beam II | 68 | 0.96 | 6558.12 | 9.61 |
| | | Beam III | 68 | 0.97 | 4254.69 | 7.74 |
| | | Beam IV | 68 | 0.98 | 2667.76 | 6.09 |

In the evaluation of the Beam II, Beam III, and Beam IV sensor locations, each sensor location exhibited a strong linearity between the recorded clean grain elevator paddle mass and output height displacement from the optical beam-based mass flow sensor. All three of the sensor locations consistently produced a coefficient of determination values greater than 0.95 across all treatment factors. However, when each sensor location was evaluated by the selected variance statistics, SSE and RMSE, Beam IV notably showed a lower variance across all crop properties and mechanical treatment factors. In the control data set, data set A, the root mean squared error was nearly half that of the other two locations. The Beam IV sensor location proved to be the ideal sensor location in comparison to the Beam II and Beam III sensor locations. The Beam IV sensor location was selected to move forward with for the evaluation of the adequate sampling frequency.

When further investigating the selected variance statistics under each treatment factor for the Beam IV sensor location, distinguishable results were able to be concluded. For example, when comparing the grain moisture content treatment factors to the control, the variance increased with the grain moisture content. The increase in variance statistics was the result of grain piling differently under each mass flow rate treatment level. The variance statistics also increased under the other crop properties treatment level where the grain test weight was manipulated independent from the crop moisture content. In data set D, where broken corn cobs were added to the grain sample, the variance statistics nearly doubled. This is speculated to be the result of a false assumption that each input grain sample would have the same percentage of broken corn cobs. When investigating the mechanical treatment factors, the variance statistics increased with clean grain elevator speed. The exact reason for the increase in that variance is unknown, but thought to be the result of settling time the grain

has on the clean grain elevator paddle before the height measurement was taken. Lastly, the variance statistics for machine orientation treatment factors were based on mechanical design and photoelectric sensor properties. In data sets H and I, when the clean grain elevator was pitch ahead and backward, respectively, the variance statistics only increase when the clean grain elevator was pitch ahead, toward the clean grain elevator chain. The interaction between the shifting grain pile on the clean grain elevator paddle and the clean grain elevator chain would add additional variance to the system from measurement to measurement. The data sets when the clean grain elevator was rolled, data sets J and K, the variance increased for both. However, in data set K, when the clean grain elevator was rolled toward the emitter, the increase in the variance statistics was the result of detectable emittance, a photoelectric sensor property. Because the beam pattern on the emitter side is significantly smaller than that of the receiver side, the shifting grain added variance to detected blockage point.

## Performance Impact of Sampling Frequency

### Tare value consistency

After identifying the optimal sensor location, Beam IV, for the placement of optical beam-based mass flow sensor, the adequate sampling frequency was identified. The output response of the Beam IV sensor location was recorded at both 2,000 Hz and 10,000 Hz. When comparing the two sampling frequencies, the standard deviation of the tare value decreased by half. The equivalent mass flow rate of the standard deviation of the tare value at a sampling frequency of 10,000 Hz was less than a tenth of a kilogram per second.

**Table 4.8 : Statistical comparison of the tare value by sampling frequency**

| Sensor | $\sigma_{tare}$ (mm) | Equivalent mass flow rate (kg/s) | Mean (mm) | Median (mm) | Standard Error (mm) |
|---|---|---|---|---|---|
| Beam IV | 0.66 | 0.17 | 41.33 | 41.77 | 0.052 |
| Beam IV_HFQ | 0.33 | 0.09 | 41.24 | 41.19 | 0.026 |

Similar to the identifying the optimal sensor location, the uncertainty in the tare value measurements were evaluated based upon the sampling frequency at the Beam IV sensor location (Table 4.9). Again, the two measurement uncertainty parameters used were repeatability and quantization error. The results from the measurement uncertainty analysis concluded that the tare values for Beam IV and Beam IV_HFQ have a standard uncertainty of 0.053 mm and 0.026 mm, respectively, at approximately a 68% confidence level.

**Table 4.9 : Tare value measurement uncertainty by sampling frequency**

| Sensor | Parameter | Source | Type | $u_{absolute}$ (mm) | Probability distribution, divisor | Standard uncertainty (mm) |
|---|---|---|---|---|---|---|
| Beam IV | Repeatability | SE | A | 0.052 | Normal, 1 | 0.052 |
| | Quantization Error | Sampling frequency | B | 0.017 | Rectangular, $\sqrt{3}$ | 0.0098 |
| | | | | Standard | Normal | 0.053 |
| Beam IV_HFQ | Repeatability | SE | A | 0.026 | Normal, 1 | 0.026 |
| | Quantization Error | Sampling frequency | B | 0.003 | Rectangular, $\sqrt{3}$ | 0.0017 |
| | | | | Standard | Normal | 0.026 |

**Treatment factors**

Increasing the sampling frequency did not substantially reduce the variance statistic under the control, data set A. However, under all the crop properties treatment factors, increasing the sampling frequency decreased both of the variance statistics. Under the mechanical treatment factors, increasing the sampling frequency did reduce the variance

statistic in five of six treatment factors. Based on the decrease to the standard deviation of the tare value and reduction in the variance statistics and measurement uncertainty, the adequate sampling frequency for the Beam IV sensor location was set at 10,000 Hz.

**Table 4.10 : Statistical comparison of treatment factor by sampling frequency**

| Data set | Treatment Factor | Sensor | n-1 | $R^2$ | SSE ($mm^2$) | RMSE (mm) |
|---|---|---|---|---|---|---|
| A | Control | Beam IV | 93 | 1.00 | 684.28 | 2.71 |
| | | Beam IV_HFQ | 89 | 0.99 | 634.34 | 2.67 |
| B | Grain moisture content | Beam IV | 65 | 0.99 | 1163.60 | 4.23 |
| | | Beam IV_HFQ | 56 | 1.00 | 674.67 | 3.47 |
| C | Grain moisture content | Beam IV | 78 | 1.00 | 768.94 | 3.14 |
| | | Beam IV_HFQ | 72 | 0.99 | 634.88 | 2.97 |
| D | Grain test weight | Beam IV | 71 | 0.98 | 3614.16 | 7.13 |
| | | Beam IV_HFQ | 65 | 0.97 | 3299.45 | 7.12 |
| E | Grain test weight | Beam IV | 60 | 1.00 | 438.58 | 2.70 |
| | | Beam IV_HFQ | 50 | 0.99 | 286.72 | 2.39 |
| F | Clean grain elevator speed | Beam IV | 65 | 1.00 | 311.31 | 2.19 |
| | | Beam IV_HFQ | 55 | 0.99 | 251.29 | 2.14 |
| G | Clean grain elevator speed | Beam IV | 74 | 0.99 | 1072.35 | 3.81 |
| | | Beam IV_HFQ | 74 | 0.99 | 974.10 | 3.63 |
| H | Machine Orientation | Beam IV | 73 | 0.99 | 1906.21 | 5.11 |
| | | Beam IV_HFQ | 68 | 0.98 | 1817.06 | 5.17 |
| I | Machine Orientation | Beam IV | 66 | 1.00 | 459.39 | 2.64 |
| | | Beam IV_HFQ | 63 | 0.99 | 432.32 | 2.62 |
| J | Machine Orientation | Beam IV | 72 | 0.99 | 1386.25 | 4.52 |
| | | Beam IV_HFQ | 64 | 0.99 | 1269.24 | 4.45 |
| K | Machine Orientation | Beam IV | 68 | 0.98 | 2667.76 | 6.09 |
| | | Beam IV_HFQ | 69 | 0.97 | 2364.25 | 5.85 |

## Conclusion

Optical beam-based mass flow sensing technologies rely heavily on the tare value height of the clean grain elevator paddle to be consistent for every measurement. In order to minimize any added mechanical variation to the tare value measurement, a new clean grain

elevator paddle was developed. The new design needed to avoid any mechanical components that would change based on lateral movement of the clean grain elevator paddle. The design in Concept #4, exemplified that quality by removing bolts heads from the measurement profile. The design featured new countersunk bolts that inset into the molded flat paddle design. Additionally, the design included a mounting bracket shield, which blocked the angled mounting bracket of the clean grain elevator paddle from the measurement. The newly designed mounting bracket shield minimized the variance in every measurement.

The optimal sensor location and adequate sampling frequency of the optical beam-based mass flow sensor was selected under both crop properties and mechanical treatment factors. Each treatment factor and level aimed to target a direct element that could influence the relationship between the collected mass of the clean grain elevator paddle and output height displacement from the optical beam-based mass flow sensor. The sensor location of Beam IV proved to have lowest variance statistics and measurement uncertainty when compared to the other two sensor locations. Additionally, when the sampling frequency of the Beam IV sensor location was increase to 10,000 Hz, the variance statistics and measurement uncertainty reduced even further. The research conducted for the optimization and selection of system components resulted in the following:

- Clean grain elevator paddle: Concept #4
- Optical beam-based sensor location: Beam IV
- Adequate sampling frequency: 10,000 Hz

The future development of an optical beam-based mass flow algorithm would utilize the optimized and selected system components from this research.

# CHAPTER 5. DEVELOPMENT OF OPTICAL BEAM-BASED MASS FLOW ALGORITHM

## Introduction

The short-term goal of this study, the identification of a relationship between the output response from an optical beam-based mass flow sensor and grain mass flowing through the clean grain elevator, was achieved in chapter 4. In order to achieve that goal, the SPTS was developed and built at Iowa State's BioCentury Research Farm. The SPTS proved to not only be an effective tool for building the relationship between the output response and grain mass flow, but also for identifying opportunities within the current design of clean grain elevator system components that could be optimized to improve the accuracy of optical beam-based mass flow sensing. A new clean grain elevator paddle was designed to reduce the variation in the tare value measurement and improve the consistency from clean grain elevator paddle to clean grain elevator paddle. Additionally, the optimal sensor placement and adequate sampling frequency of the optimal optical beam-based mass flow sensor were identified.

The focus of this chapter was to achieve the long-term goal of this study, quantifying the engineering drivers for improving the accuracy of an optical beam-based yield monitor. In order to achieve that goal, the sensor characteristics from the prior chapter were leveraged to develop an optical beam-based mass flow algorithm. The key research objectives for the development of an optical beam-based mass flow algorithm were to:

- Develop an algorithm from the data sets built on the SPTS during the experimentation in chapter 4.
- Collect field data with the system outlined in chapter 4.

- Assess the initial performance of that algorithm built from the SPTS to field data and identify the advantages and failure modes of the algorithm.
- Evaluate the accuracy and consistency of the algorithm to current yield monitoring technologies under the treatment factor of mass flow.

## Materials and Methods

### Development of Mass Flow Algorithm

#### Development from SPTS

Risius (2014) concluded that while testing in a controlled environment, like a test stand, individual treatment factors could be effectively administered throughout testing and produce distinguishable results. Risius stated that development on a test stand helped minimize any experimental biasing that could not have be avoided during field testing. Additional, the test stand accelerated understanding between the interactions of individual treatment factors and yield monitor performance. Lastly, Risius deduced that the results between the test stand and field data proved to be statistically different but correlated. This study leveraged that knowledge, different but correlated, and used the data sets produced from the SPTS in chapter 4 to develop an optical beam-based mass flow algorithm. It was anticipated that the optical beam-based mass flow algorithm would require a SPTS to field data calibration.

#### Linear regression

The 11 SPTS data sets from chapter 4 were compiled into a single data set consisting of 746 displacement and mass data points. Because the optical beam-based mass flow sensor is a volumetric sensing technology, the mass data points were converted to volume data points by dividing by the grain test weight. Due to the high coefficients of determination to a

linear curve fits in chapter 4, a linear regression was applied to the new displacement and volume data set (Table 5.1, Equation 5.1).

**Table 5.1 : Linear regression equation coefficients ANOVA**

| Coefficient | Units | Coefficients | Standard Error | t Stat | P-value |
|---|---|---|---|---|---|
| $\beta_1$ | $m^3$ / mm | 2.5E-05 | 1.9E-07 | 130.8 | 0 |

**Equation 5.1 : Linear regression clean grain elevator paddle mass estimation**

$$Clean\ grain\ elevator\ paddle\ mass\ (kg) = Height_{EFFECTIVE}\ (mm) * \beta_1 \left(\frac{m^3}{mm}\right) * Grain\ test\ weight\ \left(\frac{kg}{m^3}\right)$$

The analysis of variance tested the hypothesis that $\beta_1$ did not equal zero against the null hypothesis that $\beta_1$ did equal zero (Table 5.2). The results from that test exhibited that the probability of observing a value greater than or equal to the F statistic, 17113.9, was less than 0.05. There was strong evidence to suggest that $\beta_1$ was not equal to zero. Additionally, the coefficient of determination indicated that 95.8% of the variability in the response could be explained by the displacement measurement.

**Table 5.2 : Linear regression analysis of variance**

| Source | DF | SS | MS | F | Significance F |
|---|---|---|---|---|---|
| Regression | 1 | 6.2E-04 | 6.2E-04 | 17113.9 | 0 |
| Error | 744 | 2.7E-05 | 3.6E-08 | | |
| Total | 745 | 6.5E-04 | | | |

**Piecewise regression**

Upon further investigation of the residuals from the linear regression, the residuals were found to not have a uniform scatter. At lower displacement values, the linear regression significantly overestimated the response. At higher displacement values, the linear regression

underestimated the response. For example, plotting the control data set displacements from chapter 4 against recorded clean grain elevator paddle mass, the relationship appeared to have a distinguishable slope change at approximately 50 mm, verifying the trends found in the residuals (Figure 5.1). A piecewise regression, with one break point at 50 mm, was then developed from the displacement and volume data set (Table 5.3). A lower regression was developed from all displacement values less than 50 mm and an upper regression was developed from all displacement values 50 mm and above (Equation 5.2). The piecewise regression was modeled to reduce the error caused from the distinct slope change at low displacement values.

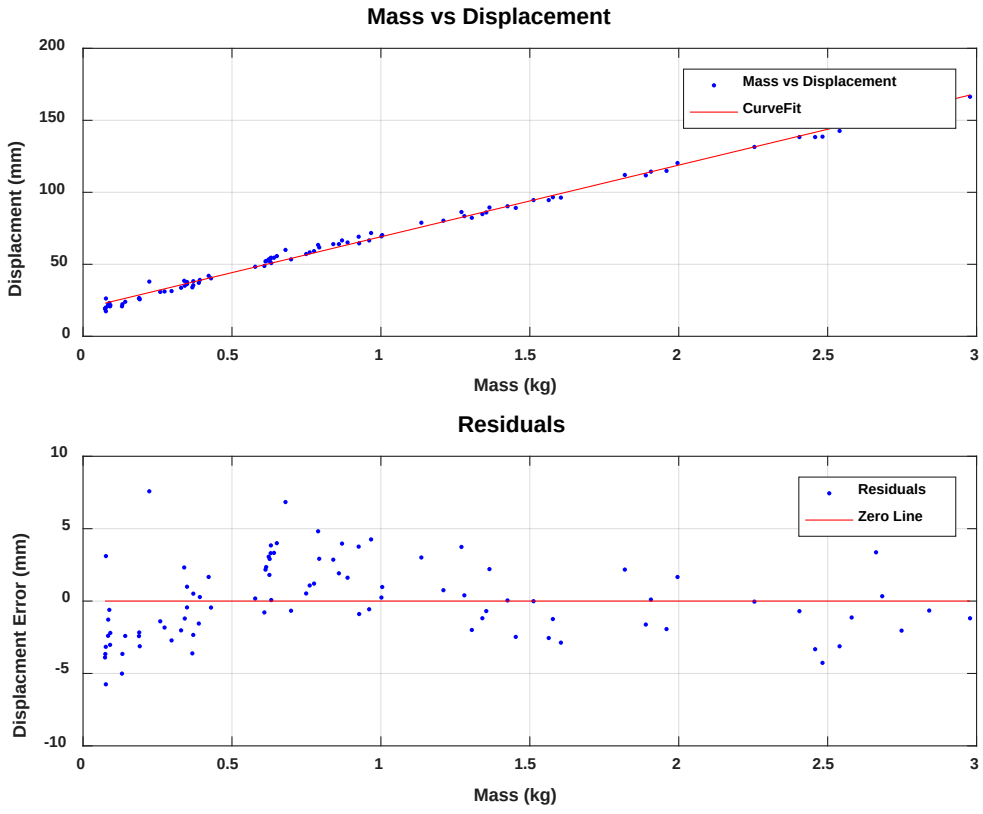


**Figure 5.1 : Linear regression residuals from chapter 4 data set A**

**Table 5.3 : Piecewise regression equations coefficients ANOVA**

| Regression | Coefficient | Units | Coefficients | Standard Error | t Stat | P-value |
|---|---|---|---|---|---|---|
| Lower | $\beta_1$ | $m^3$ / mm | 1.6E-05 | 7.1E-07 | 22.5 | 0 |
| Upper | $\beta_1$ | $m^3$ / mm | 2.5E-05 | 3.1E-07 | 79.9 | 0 |

**Equation 5.2 : Piecewise regression clean grain elevator paddle mass estimation**

$$Clean\ grain\ elevator\ paddle\ mass\ (kg)$$

$$= \begin{cases} Height_{EFFECTIVE}\ (mm) * \beta_{1_{Lower}} \left(\frac{m^3}{mm}\right) * Grain\ test\ weight\ \left(\frac{kg}{m^3}\right), & Height_{EFFECTIVE}\ (mm) < 50 \\ Height_{EFFECTIVE}\ (mm) * \beta_{1_{Upper}} \left(\frac{m^3}{mm}\right) * Grain\ test\ weight\ \left(\frac{kg}{m^3}\right), & Height_{EFFECTIVE}\ (mm) \geq 50 \end{cases}$$

An analysis of variance test was also conducted on the lower and upper regressions of the piecewise regression to test the hypothesis that the $\beta_1$ did not equal zero against the null hypothesis that $\beta_1$ did equal zero (Table 5.4). The results from both tests demonstrated that the probability of observing a value greater than or equal to either F statistic was less than 0.05. There was strong evidence to suggest that the $\beta_1$ for the lower and upper regressions of the piecewise regression were not equal to zero. The coefficients of determination for the lower and upper regressions indicated that 65.1% and 93.1% of the variability in the response could be explained by the displacement measurement, respectively.

**Table 5.4 : Piecewise regressions analysis of variance**

| Regression | Source | DF | SS | MS | F | Significance F |
|---|---|---|---|---|---|---|
| Lower | Regression | 1 | 6.3E-06 | 6.3E-06 | 504.6 | 0 |
| | Residual | 270 | 3.4E-06 | 1.3E-08 | | |
| | Total | 271 | 9.7E-06 | | | |
| Upper | Regression | 1 | 2.9E-04 | 2.9E-04 | 6388.6 | 0 |
| | Residual | 472 | 2.2E-05 | 4.6E-08 | | |
| | Total | 473 | 3.1E-04 | | | |

## Field data collection

### Combine harvester

The collection of field data was accomplished in the fall 2017. A portion of an Iowa State University research field was sectioned off specifically for this field data collection. The field data collection was completed using a John Deere S670 combine harvester equipped with two fully functional yield monitor systems, Ag Leader and Raven Industries. The factory installed Ag Leader yield monitor utilized an impact-based mass flow sensor that output its predicted mass flow rate over CAN. The Raven Industries yield monitor utilized the optical beam-based mass flow sensor and location outlined in chapter 4 (Figure 5.2). Because the Raven Industries yield monitor was an aftermarket installation, it did not have the capacity to communicate over CAN.

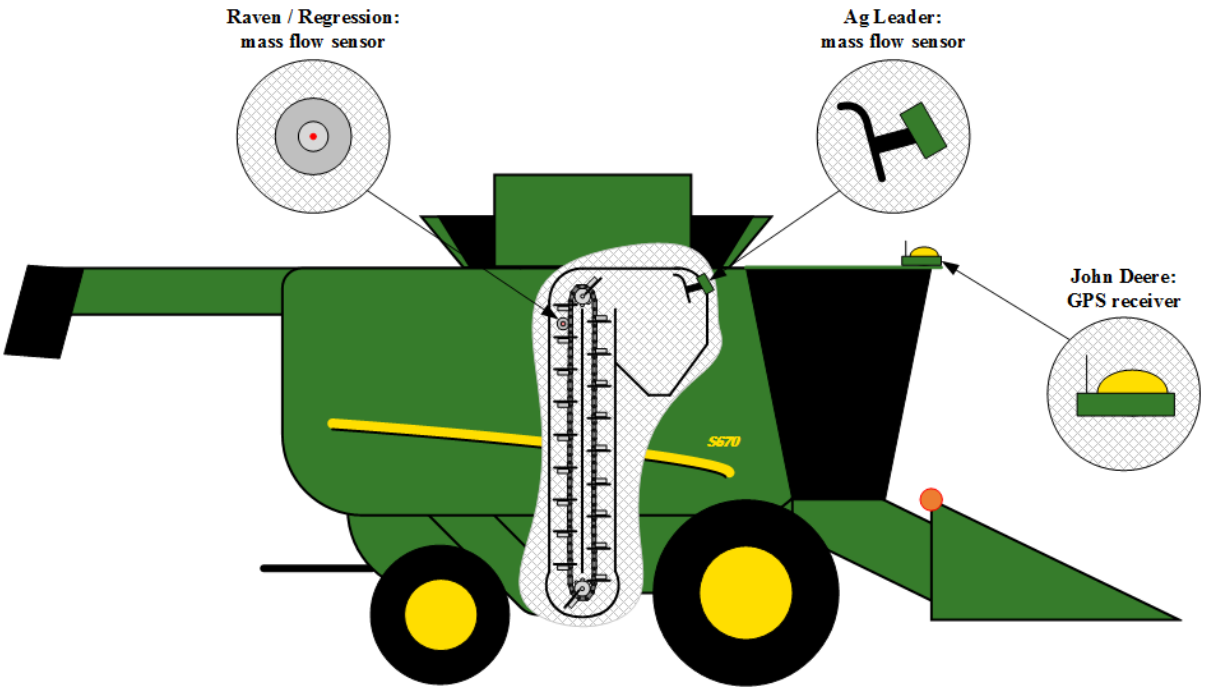


**Figure 5.2 : John Deere S670 with GPS receiver and mass flow sensor locations**

**Data acquisition system**

The data acquisition system used for the field data collection was the same NI cRIO-9038 used on the SPTS. The 8 module chassis was utilized for collecting various digital, high frequency, analog, and CAN signals. Also like the SPTS, a LabVIEW program was developed to interactively link with NI cRIO to control the starting and stopping of data logging on the combine harvester. The primary signals logged from the combine harvester were the:

- Impact-based mass flow sensor filtered output
- Optical beam-based mass flow sensor raw output
- Grain moisture content
- Pitch Angle
- Roll Angle
- Clean grain elevator speed

- Threshing system status

**Experimentation and experimental design**

The focus of the experimentation during field data collection was dictated by controllable treatment factors. Unlike on the SPTS, the grain moisture content, grain test weight, clean grain elevator speed, and machine orientation were limited by the crop properties, machine parameters, and field terrain, respectively. The only treatment factor selected for the field data collection was grain mass flow. The grain mass flow treatment levels were dictated by varying the speed of the combine harvester during harvesting operation. The limitation of the grain mass flow treatment levels were the uncontrollable inconsistencies in the crop within the field. The crop inconsistencies were estimated to significantly increase the variability within a single number targeted mass flow treatment levels. Therefore the treatment factor was extend to grain mass flow ranges with five treatment levels (Table 5.5).

**Table 5.5 : Field data collection grain mass flow range treatment levels**

| Treatment level: targeted mass flow range (kg/s) | Approximate combine harvester speed (mph) |
|---|---|
| 5-10 | 1.0 |
| 10-15 | 1.5 |
| 15-20 | 2.0 |
| 20-25 | 2.5 |
| 25-30 | 3.5 |

The goal of the experimental design for the field data collection was to produce data sets that could be used to evaluate the performance of the linear and piecewise regressions against current yield monitors in the same corn field, nonintrusive to the other yield monitors. The experimental design for the field data collection utilized the randomization of selected

grain mass flow range treatment levels. The evaluation of each randomly selected grain mass flow range treatment level produced a data set. The procedure for each data set was to:

1. Verify the combine harvester grain tank was empty.
2. Zero Raven Industries yield monitor load total.
3. Start data logging programs.
4. Begin harvesting operation with combine harvester.
5. Continue harvesting operation until approximate grain cart load size was greater than 3,000 kg.
6. Stop harvesting operation, unload combine harvester grain tank on calibrated grain cart.
7. Record Raven Industries yield monitor and calibrated grain cart load totals.
8. Stop data logging programs.

A calibrated J&M 1250 grain cart was used for the ground truth measurement for each grain mass flow range treatment level. The grain cart was calibrated to a certified truck scale at Iowa State's BioCentury Research Farm. The grain cart's calibration was verified at the end of the field data collection to check for experimental biasing. The results from that verification process found that the mean error when filling and emptying the grain cart was 0.02% and -0.3%, respectively. For this study, the J&M 1250 grain cart was determined to be an acceptable ground truth.

**Methodology for Evaluation of Algorithm Performance**

The accumulation of the mass flow rate output from Ag Leader impact-based mass flow sensor was used for the Ag Leader yield monitor data set load weight. The Raven Industries yield monitor automatically totaled its mass flow rate outputs and provided its load weight. The output from the optical beam-based mass flow sensor was recorded at 10,000 Hz

frequency and post-processed to determine the height of grain on each clean grain elevator paddle for the linear and piecewise regressions. The sums of the clean grain elevator paddle masses from the regressions were used as their load weights. The four load weights were evaluated against the grain cart load weight. The performance of each system was evaluated using three statistics from the estimated error against the ground truth measurement. The three evaluation statistics were the:

- Estimated mean error across all data sets.
- Standard deviation in the estimated error across all data sets.
- Estimated mean error per mass flow range.

## Results and Discussion

### Signal Processing

#### Tare value

Outlined in chapter 4, the tare value or empty height of the clean grain elevator paddle is pivotal part of the optical beam-based mass flow sensor's accuracy. The tare value for the field data collection was estimated by identifying sections of data sets that no mass flow was present and taking the mean of thousands of empty clean grain elevator paddle heights. The tare value used for the field data collection was estimated to be 43.2 mm. The tare value was then subtracted off every optical beam-based mass flow sensor output displacement measurement.

#### Machine orientation compensation

In U.S. Patent No. 6,282,967, CLAAS highlighted the importance of accurately determining the volume of material on a continuously conveyed blade through a conveyer shaft by the use of the combination of three photoelectric devices. CLAAS claimed to use those three photoelectric devices to determine the average depth of material on the conveyed

blade. This study only used one set of photoelectric devices, the optical beam-based mass flow sensor, and the machine orientation, provided by the GPS receiver, to determine the effective height of grain on the clean grain elevator paddle. When the machine orientation of the combine harvester was either pitched or rolled, the grain pile on the clean grain elevator paddle shifted accordingly (Figure 5.3).

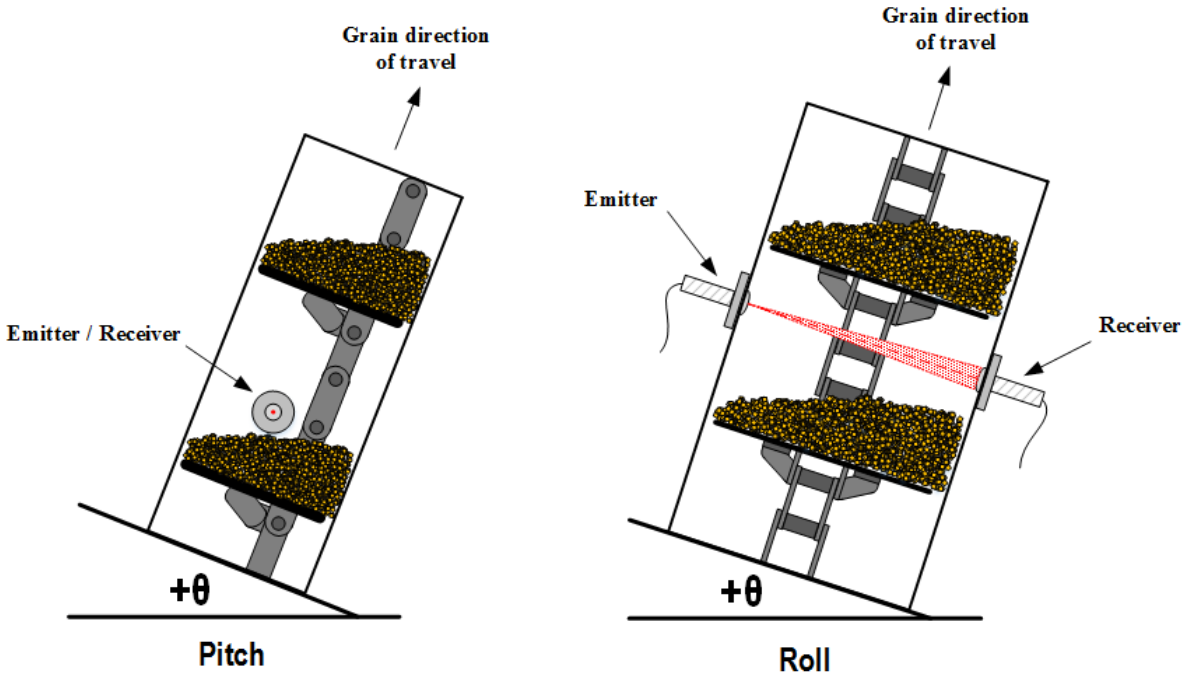


**Figure 5.3 : Result of machine orientation on clean grain elevator paddle grain pile**

The theory of compensating for machine orientation was to minimize random variation from the shifted grain pile. Determining the effective height of grain was accomplished by using the machine orientation angles and trigonometry to estimate the void sections of the grain pile (Figure 5.4).

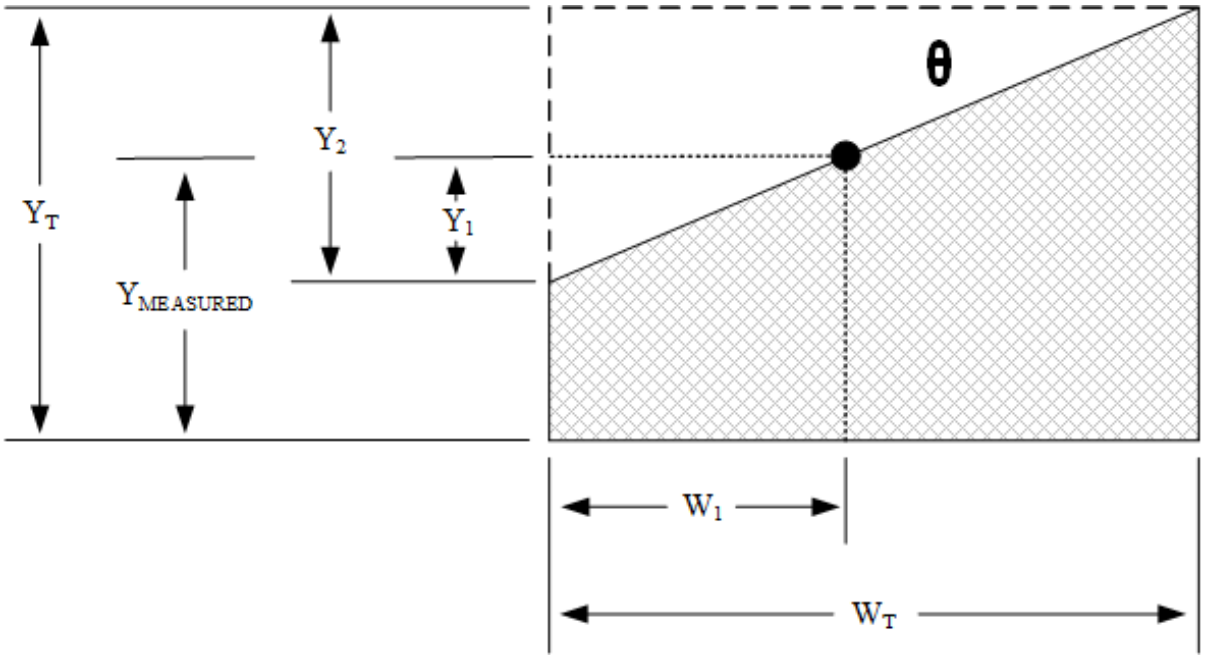


**Figure 5.4 : Theory of machine orientation compensation**

**Equation 5.3 : Complete machine orientation compensation**

$$Height_{EFFECTIVE} = Y_{MEASURED} - Tare\ value + \tan(|\theta_P|)\left(\frac{1}{2}(W_{T_P}) - W_{1_P}\right) - \frac{1}{2}\left(W_{T_R}\right)\tan(|\theta_R|)$$

The complete machine orientation compensation assumed the following:

- The grain pile completely filled the length and width of the clean grain elevator paddle.
- The inclination of the grain pile on the clean grain elevator paddle matched combine harvester's machine orientation.
- Positive and negative pitch and roll angles had the same effect on the output from the optical beam-based mass flow sensor.

### Averaging filter

In order to further minimize random variability in the grain height measurement, the pitch angle, roll angle, and clean grain elevator speed were averaged over time. Each signal utilized a 35 point moving average, the same number as the number of clean grain elevator paddles in the combine harvester (Figure 5.5). The result of the averaging filtering reduced the standard deviation of the estimated percent error in both the linear and piecewise regressions across all data sets. The limitation of the averaging filter was the loss in the instantaneous ability of the regressions to detect drastic machine changes. However, due to the large sample size of clean grain elevator paddles per data set, the averaging filter was determined to be effective and beneficial.

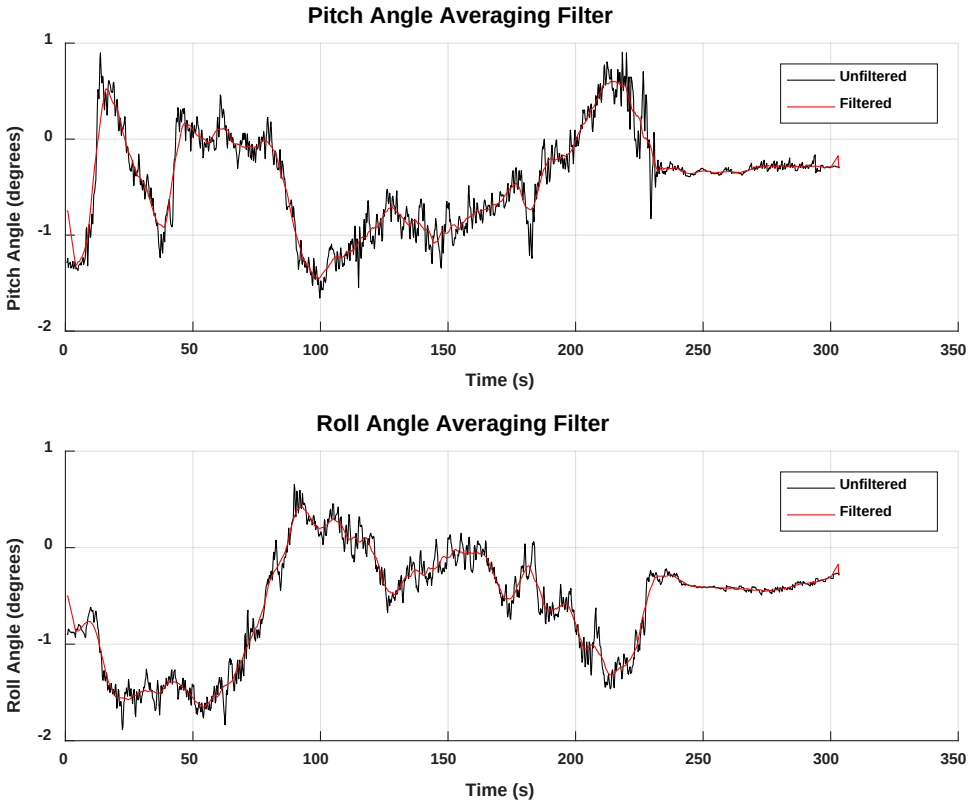


**Figure 5.5 : Averaging filter effect on pitch angle and roll angle signals**

### SPTS to field calibration

The linear and piecewise regressions developed from the SPTS were directly applied to the averaged and machine orientation compensated field data sets. The results from both of the regressions exhibited an estimated mean error across all data sets of approximately -11%. The -11% biasing estimated mean error was attributed to the expected SPTS to field data correlation and crop properties varying from that used to develop the regressions. The distribution of the mean grain moisture content per data sets from the field data collection was approximately 2% higher than that from the majority of the data sets on the SPTS. During the field data collection, several grain samples were collected to evaluate the grain test weight. The results from those grain samples processed by a GAC 2500 grain properties analyzer concluded that the mean grain test weight was 57.2 lb/bu, which was used to convert the linear and piecewise regressions volumetric output to mass. It was determined that using the mean grain test weight for field data collection was not advantageous to the linear and piecewise regressions because a field calibration would have compensated for the difference had the standard grain test weight of corn had been used.

In order to not provide any competitive advantage to the linear and piecewise regressions when comparing them against the Ag Leader and Raven Industries yield monitors, both regressions were calibrated not based on the estimated mean error across all data sets but from the estimated mean error from the same data set that the Raven Industries yield monitor was calibrated on.

## Algorithm Performance

In order to produce data sets that could be used to evaluate the performance of the two regressions against the two other installed yield monitors, grain mass flow range treatment levels were randomized to produce 34 data sets (Figure 5.6). The mass flow ranges

for each data set were produced by dividing the grain cart load weight by the estimated harvest time.

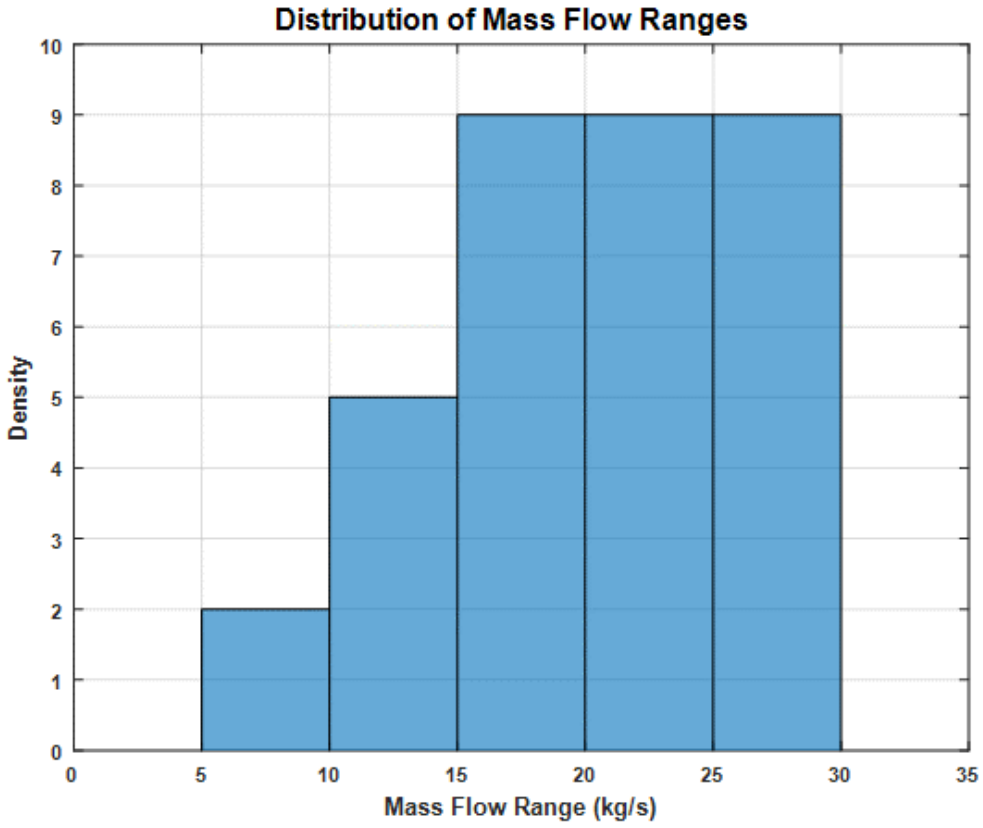


**Figure 5.6 : Distribution of the mass flow ranges**

**Estimated error across all data sets**

The analysis of the linear and piecewise regressions' estimated error statistics across all data sets produced positive results for the linear and piecewise regressions (Table 5.6). The linear regression estimated mean error across all data sets was approximately 0% and the standard deviation in the estimated error across all data sets was 5.9%. The piecewise regression estimated mean error across all data sets was slightly larger than the linear regression at 0.2%. However, the standard deviation in the estimated error across all data for the piecewise regression was 1.4% lower than that of the linear regression. In comparison to

the Ag Leader and Raven Industries yield monitors, the piecewise regression produced a lower estimated mean error and standard deviation across all data sets, but its estimated mean error was not found statistically different from either of the other two systems. The linear regression produced a lower estimated mean error than the piecewise regression but exhibited a larger standard deviation. In this study, a lower standard deviation in the estimated error was determined to be a more desirable characteristic of the yield monitor because the estimated mean error could utilize an automatic calibrated system, like John Deere's Active Yield, to atone for the mean error.

**Table 5.6 : Estimated error statistics across all data sets**

| Yield monitor | Mass flow range (kg/s) | Estimation Error | | | Tukey Grouping | |
|---|---|---|---|---|---|---|
| | | Mean | Standard Deviation | 95% CI | | |
| Linear Regression | 5-30 | 0% | 5.9% | (-2.0%, 2.0%) | A | B |
| Piecewise Regression | | 0.2% | 4.5% | (-1.9%, 2.2%) | A | B |
| Raven Industries | | 1.0% | 5.6% | (-1.1%, 3.1%) | | B |

**Mass flow range estimated mean error**

The analysis of the estimated mean error produced per mass flow range showed tangible results based on each yield monitor's algorithm. The results from the analysis exemplified the benefit of a piecewise regression when using an optical beam-based mass flow sensor (Figure 5.7). The linear regression produced increasingly higher estimated mean error at lower mass flow ranges; similar trends were exhibited by the Raven Industries yield monitor. Additionally, the Ag Leader yield monitor struggled at lower mass flow ranges.

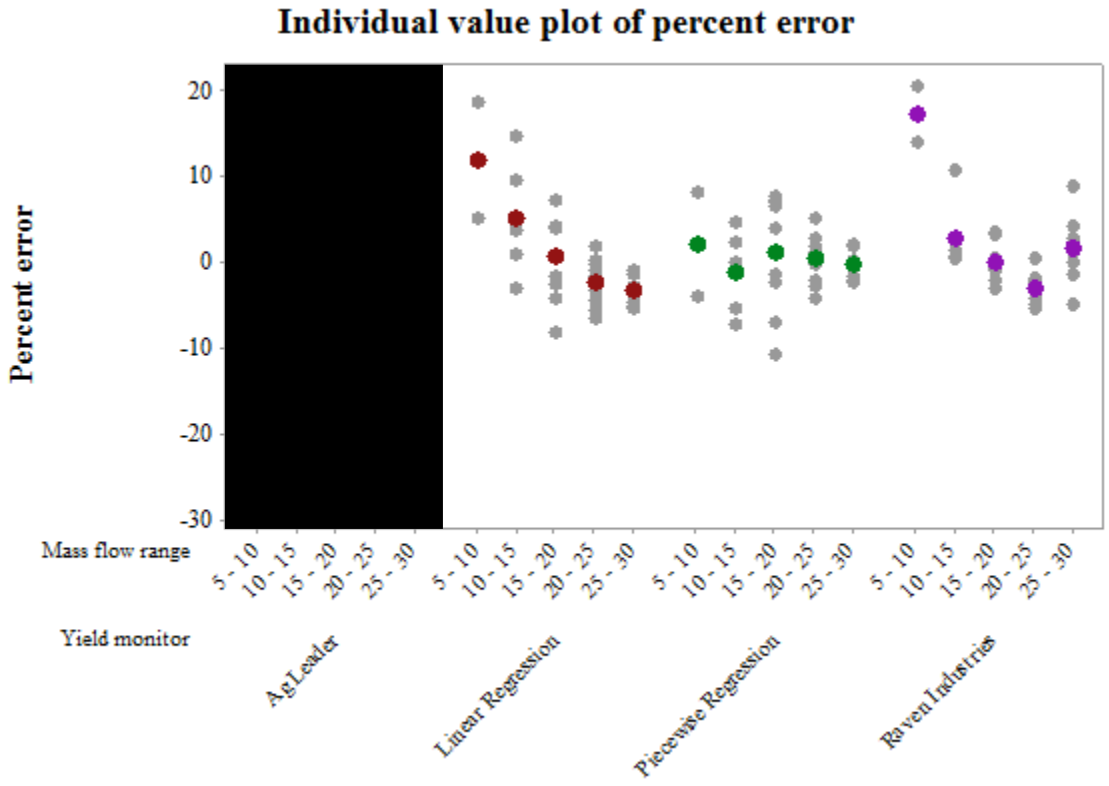


**Figure 5.7 : Yield monitor mass flow range individual value plot of error**

In the 5-10 mass flow range, the piecewise regression produced an estimated mean error of 1.9% (Table 5.7). In that same 5-10 mass flow range, the Ag Leader and Raven Industries yield monitors' estimated mean errors were [redacted] and 17.0%, respectively. However, the piecewise regression was only found statistically different from the Raven Industries yield monitor in that 5-10 mass flow range, with 95% confidence. Despite the piecewise regression producing a lower estimated mean error in all five mass flow ranges, there was no statistical difference found between it and the Ag Leader yield monitor. The Raven Industries yield monitor was found not to be statistically different from the piecewise regression in any of the mass flow ranges.

**Table 5.7 : Estimated error statistics per mass flow range**

| Mass flow range (kg/s) | N | Yield monitor | Estimation Error | | | Tukey Grouping | | |
|---|---|---|---|---|---|---|---|---|
| | | | Mean | Standard Deviation | 95% CI | | | |
| 5-10 | 2 | Linear Regression | 11.7% | 9.5% | (-2.0%, -25.4%) | | B | |
| | | Piecewise Regression | 1.9% | 8.7% | (-11.8%, 15.6%) | A | B | |
| | | Raven Industries | 17.0% | 4.6% | (3.3%, 30.8%) | | B | |
| 10-15 | 5 | Linear Regression | 5.0% | 7.0% | (-0.8%, 10.8%) | A | | |
| | | Piecewise Regression | -1.2% | 5.0% | (-7.0%, 4.6%) | A | | |
| | | Raven Industries | 2.6% | 4.4% | (-3.2%, 8.4%) | A | | |
| 15-20 | 9 | Linear Regression | 0.6% | 5.3% | (-2.7%, 3.9%) | A | | |
| | | Piecewise Regression | 1.1% | 6.9% | (-2.2%, 4.4%) | A | | |
| | | Raven Industries | -0.1% | 2.5% | (-3.8%, 3.7%) | A | | |
| 20-25 | 9 | Linear Regression | -2.4% | 2.8% | (-4.1%, -0.8%) | A | B | |
| | | Piecewise Regression | 0.3% | 3.0% | (-1.3%, 1.9%) | A | B | |
| | | Raven Industries | -3.2% | 1.8% | (-4.8%, -1.6%) | | B | |
| 25-30 | 9 | Linear Regression | -3.5% | 1.5% | (-5.4%, -1.5%) | A | B | |
| | | Piecewise Regression | -0.5% | 1.6% | (-2.5%, 1.5%) | | B | C |
| | | Raven Industries | 1.5% | 3.8% | (-0.4%, 3.5%) | | | C |

The standard deviation in the mass flow ranges was also estimated for each of the mass flow ranges. The analysis of the standard deviation in the mass flow ranges demonstrated the need to further test and develop the piecewise regression. The piecewise regression produced a higher standard deviation in the estimated mean error in four of the five ranges compared to the Ag Leader yield monitor and in all five ranges compared to the Raven Industries yield monitor.

## Conclusion

The focus of this chapter was to quantify the engineering drivers for improving the accuracy of an optical beam-based yield monitor. In this study, under the mass flow range treatment levels, the linear and piecewise regressions produced results that demonstrated an increase in the accuracy of the yield data produced from the mass flow sensor. However, the linear regression estimated mean error per mass flow range solidified the limitation of using a linear regression at lower mass flow ranges by producing increasing error. The piecewise regression, with one break point, utilized the separation of the lower and upper mass flow ranges to reduce the estimated mean error not only at lower mass flow ranges but the upper mass flow ranges as well. The piecewise regression's estimated mean error across all data sets and the standard deviation in the estimated error across all data sets was less than the current impact-based yield monitor. Additionally, the piecewise regression produced a lower estimated mean error in every mass flow range. The limitation of the piecewise regression was exhibited by higher variation in the estimate mean error for four of the five selected mass flow rate treatment levels compared to the current impact-based system. In comparison to the Raven Industries yield monitor, the piecewise regression produced an estimated mean error across all data sets, standard deviation in the estimated error across all data sets, and four of the five estimated mean error per mass flow range lower.

# CHAPTER 6. CONCLUSION

## Volumetric yield sensing in a combine harvester

Precision agriculture technologies are the source for data driven decisions that help producers receive higher returns on investments. The yield monitor provides the producers with a ground truth to the management decisions made throughout the year. The accuracy of those management decisions requires the yield monitor to be accurate. The long-term goal of this study was to quantify the engineering drivers for improving the accuracy of an optical beam-based yield monitor to increase the opportunity for producers to better manage their farming operation. The results from this study concluded that an optical beam-based mass flow sensor, utilizing a piecewise regression algorithm, optimized clean grain elevator paddle, optimized sensor location, and 10,000 Hz sampling frequency, could be a viable solution for a more accurate yield monitor.

## Suggestions for Future Testing

The SPTS proved to be an effective tool for rapidly producing data sets to characterize the effect that individual treatment factors had on the relationship between grain mass flow rate the output displacement from the optical beam-based mass flow sensor. The SPTS provides the capabilities to isolate individual treatment factors and also test the interaction of multiple individual treatment factors. Future testing on the SPTS should further the finding from this study and study the effects of applying multiple treatment factors at once has on the relationship between grain mass flow rate and the output displacement from the optical beam-based mass flow sensor. The selection of the optimal optical beam-based mass flow sensor placement was determined through four predetermined positions. Future testing should further investigate the location. Additionally, it is known that photoelectric

sensor's beam pattern can affect the performance of an optical beam-based mass flow sensor. Understanding of the limitation of misalignment from manufacturing would be beneficial to minimize overall system error. Mechanical wear is another element that can introduce error into the overall system. Mechanical wear is unavoidable in any part of a combine harvester. The harsh dynamic environment inside a combine harvester can cause wear to critical parts of the yield monitor. Additional testing should be conducted to understand the effect of wear on clean grain elevator paddle, clean grain elevator chain, and clean grain elevator sprocket have on the performance of an optical beam-based mass flow sensor.

The field data collection, in this study, altogether included 34 grain mass flow range treatment levels. Future testing in the field should target more grain mass flow range treatment levels. Similar to the SPTS experimental design, additional treatment factors like grain moisture content, severe machine orientation changes, and grain test weight could be achieved by early field season exposure, targeted field terrains, and machine parameters, respectively. Field data collection in the future should also target multiple crops.

## Suggestions for Future Development

In the development work on the SPTS, the ability to slow the clean grain elevator speed to increase the number of sampling points per grain pile on the clean grain elevator showed to reduce the variation in the output displacement of the optical beam-based mass flow sensor. For crops with reduced average mass flow rates, similar to soybeans, wheat, and canola, a clean grain elevator speed of 420 rpm might not be required. Future development work should target the reduction of the clean grain elevator speed to increase the grain pile per clean grain elevator paddle, reducing the variation in the output displacement. Another mechanical property known to influence the performance of the optical beam-based mass flow sensor is clean grain elevator chain tension. It is known that when clean grain elevator

chain tension is not adequate additional variation can be introduced into the optical beam-based mass flow measurement. Future development should be done to design a clean grain elevator system that automatically tensions the clean grain elevator chain to the proper tension.

The optimization of the clean grain elevator paddle was done to minimize the variation in the tare value measurement of the optical beam-based mass flow sensor. Future development should focus on incorporating the mounting bracket shield into the mold of the clean grain elevator paddle. The incorporation should reduce the weight of the clean grain elevator paddle and therefore reduce the cost. The newly designed incorporated clean grain elevator paddle should be injected molded with a high strength plastic.

The photoelectric sensor used for the optical beam-based mass flow sensors were not optimized for determining the height of grain on a clean grain elevator paddle. Future development should be done to optimize the beam pattern for the distance across the clean grain elevator paddle. The ON/OFF delay times of the photoelectric sensor should be developed to determine the minimum ON/OFF delay times needed to maximize the performance of the optical beam-based mass flow sensor. Lastly, the current cost of the clear optical lens used for the optical beam-based mass flow sensor is a substantial portion of the cost of the optical beam-based mass flow sensor. A design cost analysis should be done to optimize the cost and optical beam-based mass flow sensor performance.

The selection of the break point was done based on the development on the SPTS. Future development should focus on determining the optimal break point based on the SPTS and field data. The optimization of the break point in the piecewise regression could reduce the variation in the optical beam-based mass flow sensor output about the break point

equivalent mass flow rate. With the optimized break point, the estimated percent error of the piecewise regression should be approximately linear across mass flow ranges. Future development should also be done to optimize the machine orientation compensation. The current compensation assumes that positive and negative pitch and roll angles have the same effective grain pile. Investigation for the machine orientation data sets from the SPTS suggests that both pitch and roll from positive and negative angles do not have the same effect on the relationship between optical beam-based mass flow sensor displacement measurement and mass flow rate. Lastly, grain moisture content was not included in the algorithm development of the optical beam-based mass flow sensor. Because the performance of the optical beam-based mass flow sensor relies on the grain pile on the clean grain elevator paddle to be uniform, development work should be done to understand the effect grain moisture content has on the grain pile profile on the clean grain elevator paddle.

## REFERENCES

Ascheson, J. E., Fjelstad, S. F., Prairie, D. S., 2016. *Multi-Variable Yield Monitor and Methods for the Same.* United States, Patent No. 9,410,840.

Birrell, S. J., Sudduth, K. A., Borgelt, S. C., 1996. Comparison of Sensor and Techniques for Crop Yield Mapping. *Computers and Electronics in Agriculture,* Vol. 14, pp. 215-233.

Blackmore, S., Moore, M., 1999. Remedial correction of yield map data. *Precision Agriculture, 1*, 53-66.

Burks, T. F., Shearer, S. A., Fulton, J. P., Sobolik, C. J., 2003. Combine yield monitor test facility development and initial monitoring test. *Applied Engineering in Agriculture, 19*(1), 5-12.

Colvin, T. S., Jaynes, D. B., Karlen, D. L., Laird, D. A., Ambuel, J. R., 1997. Yield variability within a central Iowa field. *Transactions of the ASAE, 40*(4), 883-889.

Darr, M., 2016. "Yield Monitor Systems." *DuPont Pioneer*, www.pioneer.com/CMRoot/pioneer/us/agronomy/ympocketguide.pdf.

Fereira, J., *Historical Track Record - Crop Production*, Apr. 2017, usda.mannlib.cornell.edu/MannUsda/viewDocumentInfo.do?documentID=1593.

Homburg, H., Kollmeier, K., 2001. *Apparatus for Measuring the Throughput of Material on a Conveyer.* United States, Patent No. 6,282,967 B1.

John Deere, 2017. *John Deere S Series Combines - Rotor,* https://www.youtube.com/watch?v=264BnaPXWa0

Koch, J., Strnad, M., 2017. *Yield Monitoring Apparatus, Systems, and Methods.* United States, Patent No. 9,686,914.

Leenknegt, A., Jongmans, D. W. J., Aesaert, G., Strosser, R. P., Thomas, J. D., Hillen, C. F., 2017. *Optical Tailings Sensor in Tri-Sweep Tailings Housing.* United States, Patent Application Publication No. US 2017/0311543 A1.

Lensing, K. J., 2015. Algorithm development of a multi-section crop detection system for a corn head. MS *thesis*. Ames, IA: Iowa State University, Department of Agricultural and Biosystems Engineering.

McNaull, R. P., 2016. Development of a real-time algorithm for automation of the grain yield monitor calibration. PhD diss. Ames, IA: Iowa State University, Department of Agricultural and Biosystems Engineering.

Myers, A., 1994. *Method and Apparatus for Measuring Grain Mass Flow Rate in Harvesters.* United States, Patent No. 5,343,761.

Myers, A., 2017. *Automatic Compensation for the Effect of Grain Properties on Mass Flow Sensor Calibration.* United States, Patent No. 9,714,856.

"Procedure for Sampling, Measuring and Reporting Commingled Crop in Combine Harvest of a Subsequent Crop." *ASABE Technical Information Library,* American Society of Agricultural and Biological Engineers, 1 Jan. 1970, elibrary.asabe.org/azdez.asp?JID=2&AID=29457&CID=s2000&T=2.

Rankin, M., "Understanding Corn Test Weight." *UW Extension-Fond Du Lac Co.,* 1 Jan. 2014, fyi.uwex.edu/grain/files/2009/12/CornTW09.pdf.

Reinke, R., Dankowicz, H., Phelan, J., Kang, W., 2011. A dynamic grain flow model for mass flow yield sensor on a combine. *Precision Agriculture*, Volume 12, pp. 732-749.

Risius, N. W., 2014. Analysis of combine grain yield monitoring. MS *thesis*. Ames, IA: Iowa State University, Department of Agricultural and Biosystems Engineering.

Royer, J., "Ag Leader's Industry-Leading Yield Monitor Simplifies Collecting Quality Yield Data." *Ag Leader*, 1 Aug. 2017, www.agleader.com/blog/ag-leaders-industry-leading-yield-monitor-simplifies-collecting-quality-yie/.

"QS186E | QS18 Series All Purpose Photoelectric Sensor." *Banner Engineering*, www.bannerengineering.com/us/en/products/part.61618.html.

"QS186VP6R | QS18 Series All Purpose Photoelectric Sensor." *Banner Engineering*, www.bannerengineering.com/us/en/products/part.61624.html.

Schuster, J. N., 2016. Measuring volumetric flow rate of grains through a crop harvester to improve crop yield estimation accuracy. MS *thesis*. Ames, IA: Iowa State University, Department of Agricultural and Biosystems Engineering.

Singh, R. P., Prasad, A. K., Tare, V., Kafatos, M., 2010. *Crop Yield Prediction Using Piecewise Linear Regression with a Break Point and Weather and Agricultural Parameters.* United States, Patent No. 7,702,597 B2.

Srivastava, A., *Engineering Principles of Agricultural Machines.* American Society of Agricultural Engineers, 2006.

"Terminology for Combines and Grain Harvesting." *ASABE Technical Information Library,* American Society of Agricultural and Biological Engineers, 1 Jan. 1970, elibrary.asabe.org/azdez.asp?JID=2&AID=45631&CID=s2000&T=2.

United States Department of Agriculture, "United States Department of Agriculture." *US Standards*, www.gipsa.usda.gov/fgis/usstandards.aspx.

United States Department of Agriculture Economic Research Service, "Highlights From the August 2017 Farm Income Forecast." *USDA ERS – Highlights From the Farm Income Forecast*, www.ers.usda.gov/topics/farm-econom/farm-sector-income-finacnes/highlights-from-the-farm-income-forecast/.

Wang, B., *Development of a Grain Volumetric Flow Sensor Based on Photoelectrical Principle*. 3 Feb. 2009.

"Yield Monitor Field Test Engineering Procedure." *ASABE Technical Information Library*, American Society of Agricultural and Biological Engineers, 1 Jan. 1970, elibrary.asabe.org/azdez.asp?JID=2&AID=41696&CID=s2000&T=2.

"Yield Monitor Performance Test Standard." *ASABE Technical Information Library*, American Society of Agricultural and Biological Engineers, 1 Jan. 1970, elibrary.asabe.org/azdez.asp?JID=2&AID=23562&CID=s2000&T=2.

# APPENDIX A. BEAM IV OPTICAL BEAM-BASED MASS FLOW SENSOR

## World-Beam QS18
## Models: QS18VP6R / QS186E

### Dimensions and Features

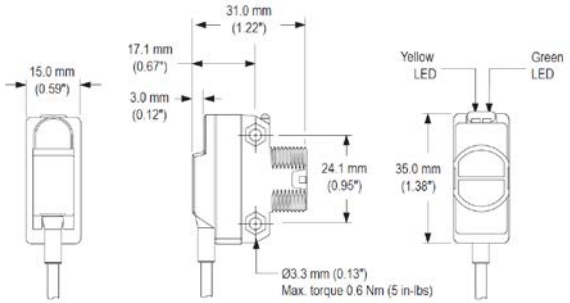


### Excess gain curve

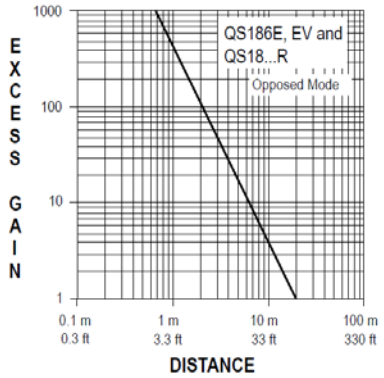


### Specifications

**Supply Voltage**
10 to 30 V dc (10% maximum ripple) at less than 25 mA, exclusive of load;
Protected against reverse polarity and transient voltages

**Light Source**
Glass Fiber Optic, Opposed and Diffuse mode models: Infrared, 940 nm
Plastic Fiber Optic, Retroreflective, Convergent and FF mode models: Visible red, 660 nm

**Adjustments**
Glass Fiber Optic, Plastic Fiber Optic, Convergent, Diffuse, and Retroreflective mode models (only): Single-turn sensitivity (Gain) adjustment potentiometer

**Indicators**
2 LED indicators on sensor top:
Green solid: Power on
Amber solid: Light sensed
Green flashing: Output overloaded
Amber flashing: Marginal excess gain (1 to 1.5x excess gain)
**Note:**Prior to date code 0223, the output indicator was red.

**Repeatability**
**Opposed Mode:** 100 microseconds
**FF Mode:** 160 microseconds
**All others:** 150 microseconds

**Output Configuration**
Solid-state complementary (SPDT): NPN or PNP (current sinking or sourcing), depending on model;
**Rating:** 100 mA maximum each output at 25 °C
**Off-state Leakage Current (FF Mode):** less than 200 µA @ 30V dc
**Off-state Leakage Current (All others):** less than 50 µA @ 30V dc
**ON-state Saturation Voltage:** less than 1 V @ 10 mA; less than 1.5 V @ 100 mA
Protected against false pulse on power-up and continuous overload or short circuit of outputs

**Output Response**
**Opposed Mode:** 750 microseconds ON; 375 microseconds OFF
**FF Mode:** 850 microseconds ON/OFF
**All others:** 600 microseconds ON/OFF
**Note:** 100 millisecond delay on power-up; outputs do not conduct during this time

**Construction**
ABS housing
3 mm mounting hardware included

**Connections**
2 m (6.5 ft) 4-wire PVC cable, 9 m (30 ft) 4-wire PVC cable, 4-pin Pico-style or Euro-style QD, 4-pin Pico-style or Euro-style 150 mm (6 in) pigtail QD, depending on model

**Environmental**
IEC IP67; NEMA 6

**Operating Conditions**
**Temperature:** –20 °C to 70 °C (–4 °F to 158 °F)
**Relative Humidity:** 90% @ 50 °C (non-condensing)

### Beam pattern

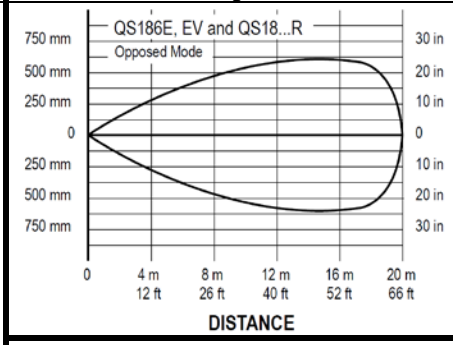


### QS18VP6R wiring diagram

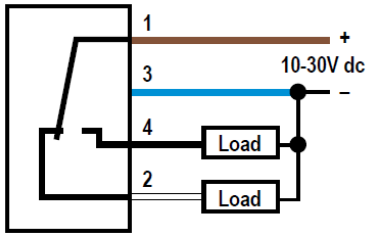


### QS186E wiring diagram

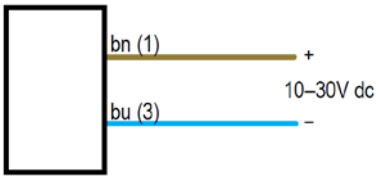


Note: this table is not an official datasheet from Banner Engineering Corp. but a modified replicate containing relavent information to this study

# APPENDIX B. MACHINE ORIENTATION COMPENSATION

## Machine Pitch Compensation

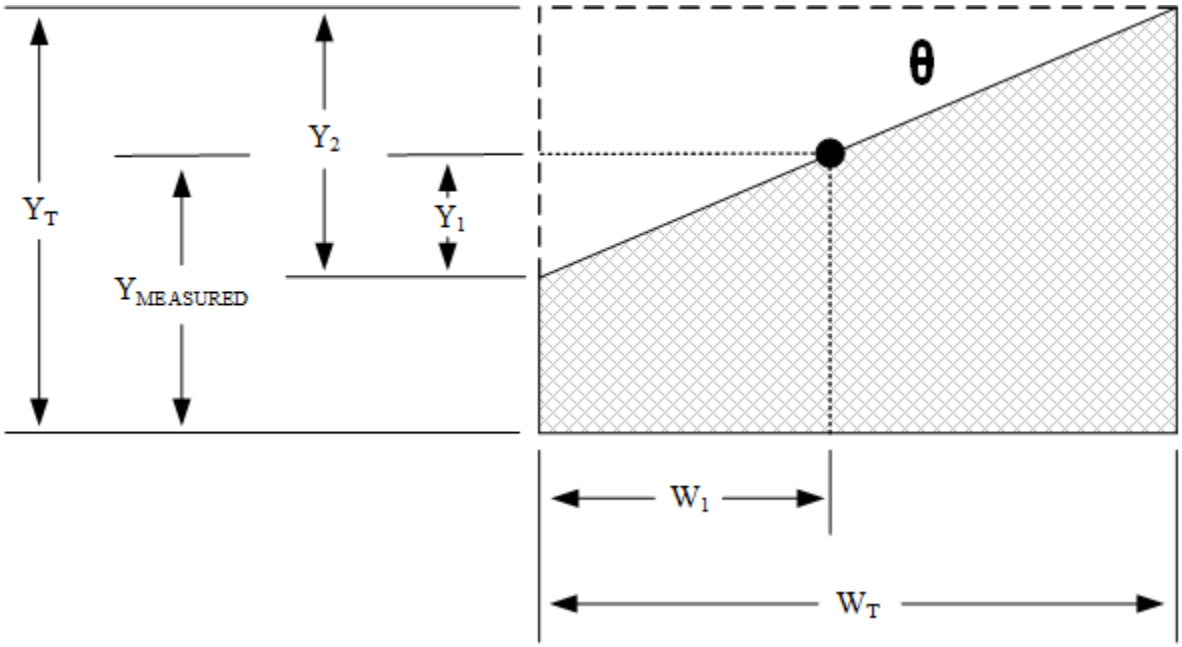


**Figure B.1 : Theory of pitch compensation**

**Equation B.1 : Equations to estimated pitch compensation**

$$Y_2 = \frac{Y_1\,(W_T)}{W_1}$$

$$Y_1 = W_1 \tan(\theta)$$

$$Y_{MEASURED} = Y_T - (Y_2 - Y_1)$$

$$Y_T = Y_{MEASURED} + (Y_2 - Y_1)$$

$$Y_T = Y_{MEASURED} + \left(\frac{Y_1\,(W_T)}{W_1} - W_1 \tan(\theta)\right)$$

$$Y_T = Y_{MEASURED} + \left((W_T)\tan(\theta) - W_1 \tan(\theta)\right)$$

$$Area_{TOTAL} = Y_T\ (W_T)$$

$$Area_{EMPTY} = \frac{1}{2} Y_2\ (W_T)$$

$$Area_{EFFECTIVE} = Area_{TOTAL} - \ Area_{EMPTY}$$

$$Area_{EFFECTIVE} = Y_T\ (W_T) - \frac{1}{2} Y_2\ (W_T)$$

$$Area_{EFFECTIVE} = Y_T\ (W_T) - \frac{1}{2}\ {W_T}^2 \tan(\theta)$$

$$Area_{EFFECTIVE} = \ W_T\ (Y_T - \frac{1}{2}\ (W_T) \tan(\theta))$$

$$Height_{EFFECTIVE} = \ Y_T - \frac{1}{2}\ (W_T) \tan(\theta)$$

$$Height_{EFFECTIVE} = Y_{MEASURED} + \big((W_T) \tan(\theta) - W_1 \tan(\theta)\big)\ - \frac{1}{2}\ (W_T) \tan(\theta)$$

$$Height_{EFFECTIVE} = Y_{MEASURED} + \tan(|\theta|) \left(\frac{1}{2} (W_T) - W_1\right)$$

**Machine Roll Compensation**

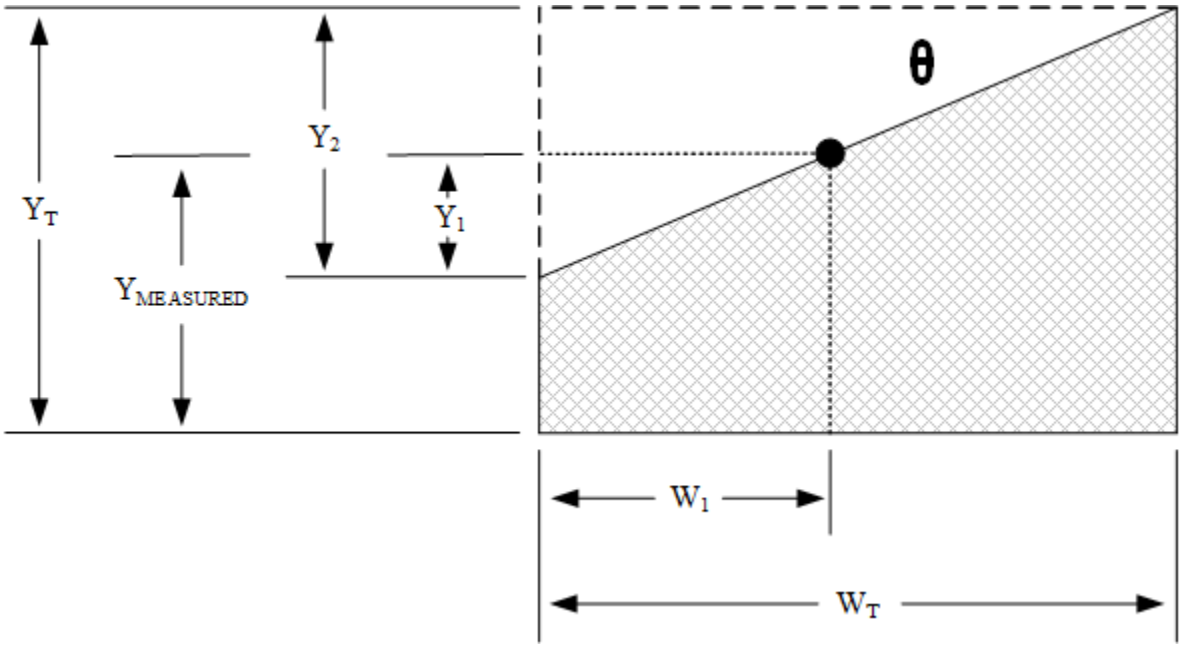


**Figure B.2 : Theory of roll compensation**

**Equation B.2 : Equations to estimated roll compensation**

$$Y_2 = \frac{Y_1\,(W_T)}{W_1}$$

$$Y_1 = W_1 \tan(|\theta|)$$

$$Y_{MEASURED} = Y_T - (Y_2 - Y_1)$$

$$Y_T = Y_{MEASURED} + (Y_2 - Y_1)$$

$$Y_T = Y_{MEASURED} + \left(\frac{Y_1\,(W_T)}{W_1} - W_1 \tan(|\theta|)\right)$$

$$Y_T = Y_{MEASURED} + \left((W_T)\tan(|\theta|) - W_1 \tan(|\theta|)\right)$$

$$Area_{TOTAL} = Y_T\ (W_T)$$

$$Area_{EMPTY} = \frac{1}{2} Y_2\ (W_T)$$

$$Area_{EFFECTIVE} = Area_{TOTAL} - Area_{EMPTY}$$

$$Area_{EFFECTIVE} = Y_T\ (W_T) - \frac{1}{2} Y_2\ (W_T)$$

$$Area_{EFFECTIVE} = Y_T\ (W_T) - \frac{1}{2}\ {W_T}^2 \tan(|\theta|)$$

$$Area_{EFFECTIVE} = W_T\ (Y_T - \frac{1}{2}\ (W_T) \tan(|\theta|))$$

$$Height_{EFFECTIVE} = Y_T - \frac{1}{2}\ (W_T) \tan(|\theta|)$$

$$Y_T = Y_{MEASURED}$$

$$Height_{EFFECTIVE} = Y_{MEASURED} - \frac{1}{2}\ (W_T) \tan(|\theta|)$$

## Complete Machine Orientation Compensation

### Equation B.3 : Complete machine orientation compensation

$$Height_{EFFECTIVE} = Y_{MEASURED} - Tare\ value + \tan(|\theta_P|)\left(\frac{1}{2}\left(W_{T_P}\right) - W_{1_P}\right) - \frac{1}{2}\left(W_{T_R}\right)\tan(|\theta_R|)$$